

T-4507

THE HYDRATION AND GEOCHEMISTRY OF SILICIC VOLCANIC GLASSES

by

James R. Piper

ProQuest Number: 10783969

All rights reserved

INFORMATION TO ALL USERS

The quality of this reproduction is dependent upon the quality of the copy submitted.

In the unlikely event that the author did not send a complete manuscript and there are missing pages, these will be noted. Also, if material had to be removed, a note will indicate the deletion.



ProQuest 10783969

Published by ProQuest LLC (2018). Copyright of the Dissertation is held by the Author.

All rights reserved.

This work is protected against unauthorized copying under Title 17, United States Code
Microform Edition © ProQuest LLC.

ProQuest LLC.
789 East Eisenhower Parkway
P.O. Box 1346
Ann Arbor, MI 48106 – 1346

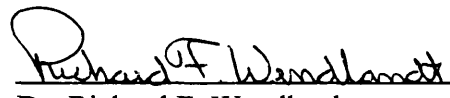
T-4507

A thesis submitted to the Faculty and Board of Trustees of the Colorado School of Mines in partial fulfillment of the requirements for the degree of Master of Science (Geology).

Golden, Colorado

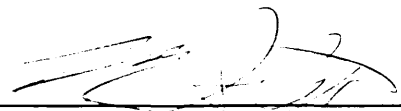
Date Nov. 11, 1994

Signed: 
James R. Piper

Approved: 
Dr. Richard F. Wendlandt
Thesis Advisor

Golden, Colorado

Date 11/12/94


Dr. Roger M. Slatt
Professor and Head,
Department of
Geology and Geological Engineering

ABSTRACT

Hydration processes, both primary and secondary, provide insight into the water speciation and water content of magmas. Polymerization of magma and incorporation of secondary water into volcanic glass are both dependent on the relative bonding strength of the hydrous species. Transmission infrared spectroscopy is used to determine how water (H_2O versus OH^-) is bound and distributed in obsidian and perlite (hydrated obsidian). A method using powdered samples in KBr pellets is used to quantify water in volcanic glasses with total or combined H_2O concentrations up to and > 2 wt.%. This technique uses independent absorption coefficients which change with the proportion of molecular to hydroxyl water. The results indicate that, at ambient temperatures and pressures, hydroxyl concentrations reach an upper limit of approximately 0.30 wt.% H_2O . Above this limit molecular water species comprise the remaining fraction of the combined water.

The distribution of water species throughout the glass can be assessed by determining the identity of the elements migrating into and out of the glass. The results demonstrate that an increase in hydroxyl and molecular water contents is accompanied by decreases in Si, Al, K, and Na. Other network modifiers, such as Ca and Mg, do not show significant change with the addition of hydroxyl or molecular water.

TABLE OF CONTENTS

	Page
ABSTRACT iii
LIST OF FIGURES vii
LIST OF TABLES ix
ACKNOWLEDGMENTS x
Chapter 1. INTRODUCTION 1
1.1 Purpose of Study - The Problem 1
1.2 Hydration of Glass 1
1.3 Mineral Constituents 4
1.4 Hydration Models 7
1.5 Geochemical Definitions 8
1.5 Neutron Magnetic Resonance & Raman Spectroscopy Concepts 12
1.6 Previous Studies 14
1.6.1 Geochemistry 14
1.6.2 Spectroscopy 23

Chapter 2. METHODS	29
2.1 Transmission Samples	29
2.2 Transmission Sample Preparation	29
2.3 Transmission Procedures	32
2.4 Transmission Calibration	33
Chapter 3. DATA	34
3.1 Geochemical Characterization	34
3.2 Water Analysis	38
3.3 Water Determinations	43
3.3.1 Method I	44
3.3.2 Method II	44
3.3.3 Method III	47
3.3.4 Unknowns	49
3.4.5 Geochemical Data	49
Chapter 4. RESULTS	55
4.1 Data Treatment	55
4.2 Data Analysis	56

4.2.1 Water Species	57
4.2.2 Network Formers	57
4.2.3 Network Modifiers	62
4.2.4 Network Modifiers : Network Former	67
Chapter 5. INTERPRETATION OF RESULTS	77
5.1 Hydroxyl Contents	77
5.2 Network Formers	78
5.3 Network Modifiers	80
5.4 Network Modifiers : Network Former	82
Chapter 6. CONCLUSION	84
REFERENCES	86

LIST OF FIGURES

	Page
1. Phase relationships at the glass-liquid interface . . .	6
2. Glass Package . . .	9
3. Hydration Model	10
4. Tetrahedral Network Configurations	15
5. Subdivisions of the Infrared Spectrum	25
6. Vibrational motions of H ₂ O	27
7. Na ₂ O + K ₂ O & CaO versus SiO ₂	36
8. Absorbance versus Manometric H ₂ O - KBr Pellets	41
9. Absorbance versus Manometric H ₂ O - Slabs	42
10. IR H ₂ O (wt.%) versus Manometric H ₂ O (obsidian)	50
11. IR H ₂ O (wt.%) versus Manometric H ₂ O (obsidian & perlite)	51
12. OH ⁻ (mole%) versus Total H ₂ O (H ₂ O + OH ⁻)	58
13. SiO ₂ (mole%) versus OH ⁻	59
14. SiO ₂ (mole%) versus H ₂ O	60
15. Al ₂ O ₃ (mole%) versus OH ⁻	61
16. Al ₂ O ₃ (mole%) versus H ₂ O	63
17. SiO ₂ + Al ₂ O ₃ (mole%) versus OH ⁻	64

18.	K ₂ O (mole%) versus OH ⁻	65
19.	K ₂ O (mole%) versus H ₂ O	66
20.	Na ₂ O (mole%) versus OH ⁻	68
21.	Na ₂ O (mole%) versus H ₂ O	69
22.	CaO (mole%) versus OH ⁻	70
23.	CaO (mole%) versus H ₂ O	71
24.	MgO (mole%) versus OH ⁻	72
25.	MgO (mole%) versus H ₂ O	73
26.	CaO+Na ₂ O+K ₂ O/Al ₂ O ₃ (mole%) OH ⁻	75
27.	CaO+Na ₂ O+K ₂ O/Al ₂ O ₃ (mole%) H ₂ O	76

LIST OF TABLES

	Page
Table I	Band Assignments 28
Table II	Sample Locations 30
Table III	Chemistry (wt.%) 35
Table IV	Absorbance/Manometric H ₂ O - Calibration Samples 40
Table V	Absorbance/Manometric H ₂ O - Unknowns 43
Table VI	Water Determinations - Method I 45
Table VII	Method II - Absorption Coefficients taken from Newman et al. (1986) 46
Table VIII	Method III - Absorption Coefficients - IR/Manometric H ₂ O 48
Table IX	Water Determinations - Unknowns 52
Table X	Chemistry - H ₂ O & OH ⁻ (mole%) 53
Table XI	Alumina Saturation 54

ACKNOWLEDGEMENTS

The author would like to express thanks to Dr. Irving Friedman of the U.S.G.S. for his recommendations and assistance in planning, obtaining samples, solving analytical problems, and interpreting the data. It was a privilege to learn from such a distinguished research scientist.

Without the expertise in editing, advice and assistance in planning from Dr. Richard Wendlandt of the Colorado School of Mines, the thoroughness and quality of this thesis would have suffered. I am indebted to him for all of the hard work he put in on the supervision of this study.

I was also very fortunate to have been allowed to use Dr. Roger Clark's equipment at the U.S.G.S. Both he and Greg Swayze helped me tremendously with instruction of how to use the Nicolet IR Spectrometer, interpret IR data, and how to use Roger's program SPECPR to analyze the spectral data.

I am most thankful for the tremendous support from my parents. Without their help I would not have been able to develop and polish this work.

I also want to thank Mary and John for having patience, and giving me the time to pursue this endeavor.

Chapter 1. INTRODUCTION

1.1 Purpose of Study - The Problem

The purpose of this investigation is to quantify the molecular water/silanol ratio in hydrated silicic volcanic glasses, to determine the processes responsible for hydration, and to examine the influence of glass chemistry upon hydration. In volcanic glasses, molecular water is defined as the H_2O species which, in addition to the OH^- species, comprises total H_2O ("combined water"). Other questions this study will help answer, which are important to the interpretation and understanding of obsidian and perlitic glasses, are below.

- 1.) How is water bound within the glass?
- 2.) What influences the distribution of water in the glass?
- 3.) Are the water species loosely or tightly bonded?
- 4.) How is water distributed structurally throughout the glass?
- 5.) What role does the distribution of water in glass have in the processes of diffusion and leaching?

1.2 Hydration of Glass

In this study, the concentrations of molecular versus hydroxyl water in obsidian,

perlite, and pitchstone are examined. The relationships between petrochemistry and hydration are examined, with the specific goal of determining the role network formers and network modifiers play in the hydration of volcanic glass.

Obsidian, a primary silicic volcanic glass associated with young (tens to hundreds of thousands of years old) silicic volcanic rocks, is commonly massive, found as the major lithologic component in dome and flow complexes. Obsidian may contain microlites, and crystallites, or pods or stringers of vapor-phase minerals. Although often dark-colored, lighter colored grey, translucent varieties are also found as nodules up to 1mm in diameter, pervasively distributed throughout a perlite matrix. The most common nodule variety found in perlite is "Apache tears," which are jet-black in color and variable in size, ranging from small grains < 1mm to spheroids several centimeters in diameter.

Water contents of obsidians range from 0.1 - 1.3 wt.%, although only a few isolated samples have been reported to have high water contents, and several of these samples were collected from the contact between volcanic domes and sediments which may have been water-saturated. A more realistic upper limit for a normal distribution is 0.3% (Friedman, 1993).

The types of juvenile water species in obsidians are not precisely known. Hydroxyl water has been interpreted to be dominant over molecular water, based upon thermodynamic data, but it is not entirely clear that molecular water is present as a juvenile constituent. Iler (1979), using thermodynamic arguments, suggested that silanol water (SiOH) should be the dominant monomer found in most natural glasses. The

hydroxyl component of silanol water is interpreted as representing juvenile magmatic water, somehow distributed throughout a network of silica tetrahedra, which exhibits no long range order. In this study the term "hydrated obsidian" includes molecular water.

Perlite, which is altered volcanic glass associated with silicic volcanic flows, has seldom been recognized and its origin is poorly understood. The fabric of perlitic glass is extremely important in establishing lithologies and spatial relations in volcanic settings. For example, the presence of "false pyroclastic textures" (Alan, 1988) has led many geologists to label some occurrences of perlite as comprising froth flows (Boyd and Kennedy, 1951; Kennedy, 1955; Boyd, 1961; McCall, 1964), tufolavas and clastolavas, (terms used by many Russian geologists; Cook, 1966), foam lavas (Locardi and Mittempergher, 1967), ignispumites (Panto, 1962), and globule lavas (Johnson, 1968).

By the traditional definition, perlite is a hydrated volcanic glass with 2 - 5% H₂O, commonly with a pearly luster and an onion-skin texture. This definition has been extended to include volcanic glasses, with textures ranging from pumiceous to granular, that are hydrated, but have perlitic fractures only visible using SEM techniques (Heiken and Woletz, 1987). Pitchstones, which have higher water content than obsidians, are characterized by a waxy dull resinous luster and may be similar to perlites. Friedman and Smith (1958) presented evidence from hydrogen isotope measurements that perlite forms by secondary hydration. During this process, meteoric waters pervasively overprint the juvenile water content of the primary glass (obsidian). Remnant cores of obsidian (Apache tears) set in a matrix of classical perlite provide evidence that hydration precedes inward

along hydration rinds towards the center of the obsidian core. Friedman and Smith (1958) propose that molecular water represents the water species incorporated into the glass during hydration. The water speciation in perlite consists of both molecular and hydroxyl components. Hydroxyl versus molecular isotopic fractions cannot be effectively separated solely based on isotopic fractionation and inferred provenance of isotopic components.

Molnar (1989) and Marakushev and Yakovleva (1980) alternatively propose that the waters of hydration in perlite originate from a primary magmatic source. This view is commonly espoused throughout much of the eastern European geologic community and has been proposed in North America by geologists including Naert (1974).

This study adopts the former hypothesis, which is discussed in section 1.4. It is beyond the scope of this study to critically analyze the alternative hypothesis, for reasons which will become apparent in the development of this text.

1.3 Mineral Constituents

Aphyric glass selvages host mineral constituents which can be classified as primary crystallization products (including primary devitrification), incipient crystallization products (crystallites formed in lavas during and after emplacement), and secondary devitrification products (formed by reactions with meteoric and connate waters). Minerals which belong to these categories are discussed below.

- 1.) Feldspar with large (800 - 1100um) partially resorbed margins found associated with quiescent lavas that crystallized at subsequent to explosive eruptions. Large (400 - 1000um), cumulophyric clumps, which suggest primary devitrification from a supercooled liquid (Figure 1), and are characterized by euhedral to subhedral micropertthitic crystals (Piper, 1991). Corrosion of crystal margins may be indicative of dissolution in response to the evolution of a volatile fluid phase in shallow seated magma reservoirs.
- 2.) Incipient crystallization of feldspar within lava flows results in the formation of crystallite (<10um) nucleation from a supercooled liquid. These crystals are trachytic and typically subhedral with corroded lath ends that resemble a feather.
- 3.) Secondary devitrification minerals found dispersed within lithophysal cavities and along axialitic structures include:
 - a.) Clay pervasively overprinting secondary feldspars in spherulitic growths.
 - b.) Zeolites found adjacent to localized concentrations of secondary clays in feldspar spherulites.
 - c.) Secondary feldspar dispersed throughout the groundmass as microlites.
 - d.) Accessory minerals, such as hematite, pervasively distributed within stringers and pods and intimately associated with finely disseminated feldspars which are produced by vapor-phase alteration.
 - e.) Hematite locally distributed pervasively throughout a groundmass of

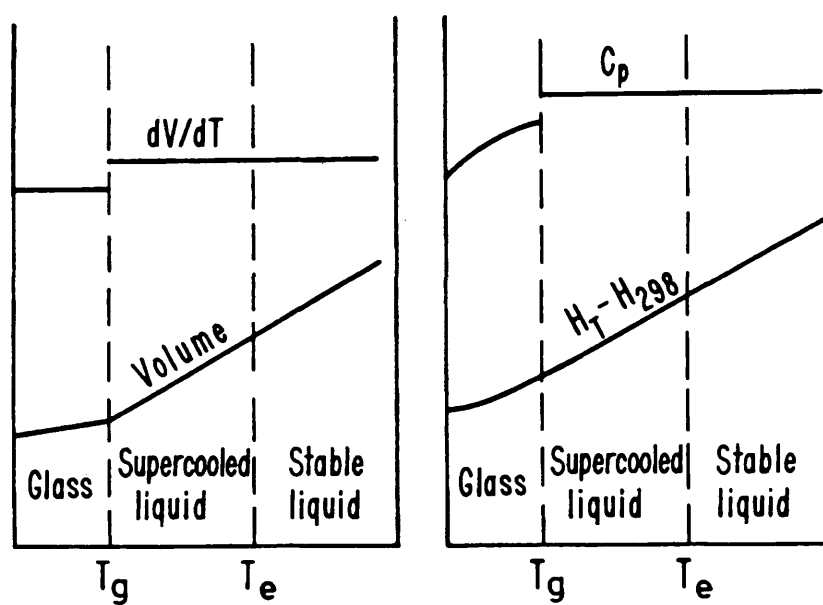


Figure 1. Phase relationships at the glass-liquid interface

Phase changes which describe the quenching of lava or magma as a function of temperature. T_e is the equilibrium temperature, and T_g is the glass transformation temperature. dV/dT is the change in volume with respect to the change in temperature, and C_p is the heat capacity at constant pressure. (Taken from Carmichael, 1979).

glass (megascopically labeled as "red stained perlite").

1.4 Hydration Models

The hydration processes presented in section 1.2, and the mineralogical characterization shown in section 1.3, were combined with surface mapping and drilling of commercial perlite deposits to produce geological glass hydration models which illustrate spatial and temporal relationships. Large scale hydration selvages, with glass thicknesses ≥ 30 m are recognized as being formed from exogenous domes and flows associated with dome/flow complexes (Whitson, 1982). The glass selvage in an exogenous dome is shown in Figure 2a. The cooling units are classified on the basis of texture and are listed as:

- 1.) Devitrified core (which includes glass and felsite)
- 2.) Classical perlite, with a pronounced onion-skin texture
- 3.) Granular perlite, with a fine grained sugary, granulated texture
- 4.) Vesicular (pumiceous) perlite, which is brecciated locally.

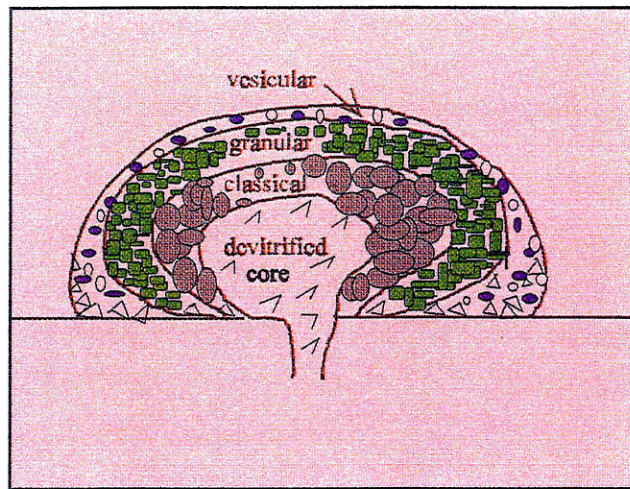
The textural variations shown in Figure 2a and 2b, demonstrate the variability in the hydration model with changing chemistry. The dome model depicts the textural variations in subaluminous lavas, while the flow model shows the textural hydration selvage and

lithologies for slightly peralkaline flows, which have low aspect ratios due to the concentrations of excess molar alkalis with respect to alumina. The significant textural difference between these two models is the presence of massive obsidian in the basal portion of peralkaline flows, just above the basal breccia (Figure 2b).

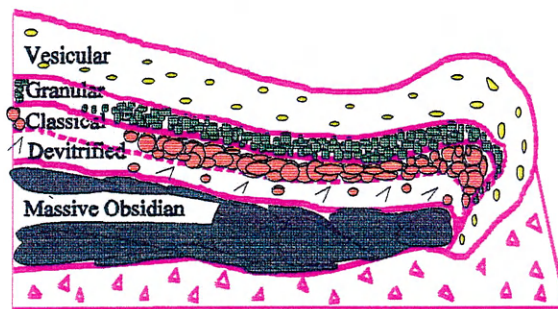
On a microscopic scale, the hydration of of obsidian to form perlite was interpreted from the presence of obsidian nodules, found as the cores of hydration cells. The hydration cells can be seen megascopically as classical onion skin perlite. The spheroidal draping of successive thin layers of perlite around obsidian nodules resembles the exfoliation of granites due to weathering. The hydration model used in this study attributes the formation of perlite as being hydration by meteoric water, introduced along fractures within the glass (Figure 3a). Molecular water is introduced along major primary fractures, and is diffused along hydration fronts which penetrate the glass along thin layers normal to the fractures. These layers or "hydration rinds" diffuse towards the central core of the mass progressively with respect to time (Figure 3b). Late stage fractures are produced in response to structural weakening of the glass which was altered from diffusive hydration (Figure 3a).

1.5 Geochemical Definitions

In order to provide a starting point from which to evaluate geochemical data presented later in this study, it is important to consider the structure of glass. This thesis

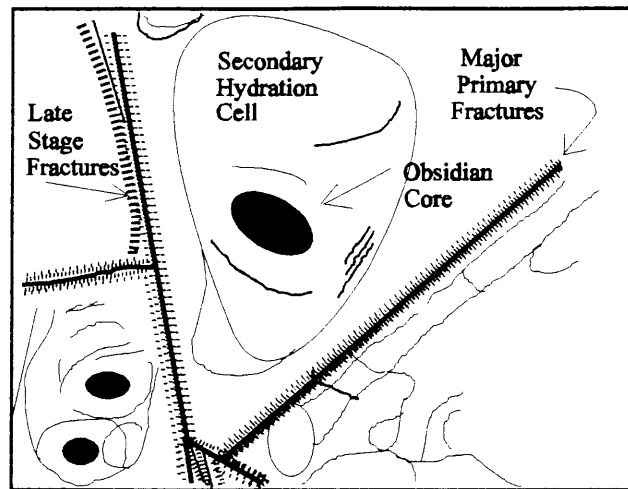


a.) Exogenous dome model. This model characterizes the subdivisions of the glass selvage by dominant texture (modified after Whitson, 1982).

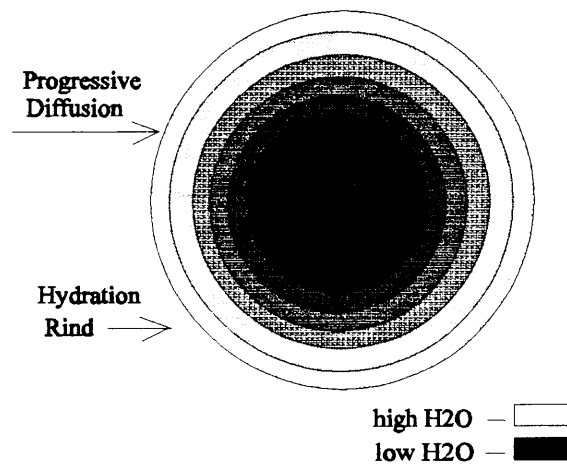


b.) Profile of a perlitized flow. A basal breccia underlies the glass package. The toe of the flow has ramp structures.

Figure 2. Glass Package



a.) Sketch of a photomicrograph of a perlite occurrence at Zey Lik, western Turkey. The secondary hydration cell is defined by secondary hydration fractures in classical onion skin perlite. The major primary fractures are conduits for molecular water. The late stage fractures develop from the weakening of the glass associated with the diffusion of water into the glass.



b.) Hydration model which shows the progressive diffusion of water into the glass.

Figure 3. Hydration Model

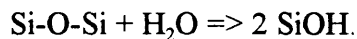
adopts the random glass network model (Ericson et al., 1976; Zachariasen, 1932) to explain the absence of periodic symmetry (short range order) in glasses when analyzed by x-ray diffraction. According to this model, glass contains silica tetrahedra that have both bridging and non-bridging oxygens. The non-bridging oxygens are randomly oriented and the gaps or holes between adjacent tetrahedra are occupied by large, low charge cations such as Na^+ , K^+ , and Ca^{+2} . These cations, known as network modifiers, are commonly octahedrally coordinated to oxygen and are soluble throughout the network. Another group, the "intermediates," behave as both network modifiers and network formers and include ions such as Al^{+3} . In high molar alumina content peraluminous glasses, aluminum behaves geochemically as a network modifier with a coordination number of 6, network former with a coordination number of 4 (Ericson et al., 1976). The tendency for aluminum to act as a network modifier decreases with decreasing molar alumina concentrations when alkali or alkaline earth elements are present in concentrations great enough to balance electrostatic valence. Aluminum where present in high proportion, occurring as a network modifier may weaken glass structure and promote rapid breakdown of the glass during hydration. The random glass network model does not define either the degree or the character of short range order.

The most important bonding relationship to consider in glasses is the ratio of non-bridging oxygens to bridging oxygens. In a melt, this ratio is important in defining the degree of polymerization. This ratio can be increased by:

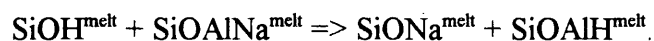
- 1.) adding large lithophile cations with low valence such as K^+ , or Na^+ ,
- 2.) adding tetrahedrally coordinated cations with a higher valence state than silicon (such as P_2O_5 or V_2O_5),
- 3.) adding a fluoride which will interfere with oxygen bridging due to its greater electronegativity, and
- 4.) adding hydroxyls.

This study will examine the relationship between large lithophile cations and hydroxyls in obsidian. Unaltered obsidian is assumed to represent the original composition of the magma.

The basic hydration reaction which occurs in a melt is



This reaction was employed in the cation exchange model for albitic melts developed by Burham (1975) and can be rewritten as



This ideal water-magma mixing reaction sets the stage to examine relationships between hydroxyl concentrations and tetrahedrally coordinated cations in obsidian.

1.5 Neutron Magnetic Resonance & Raman Spectroscopy Concepts

A comprehensive review of glass theory is beyond the scope of this study. The

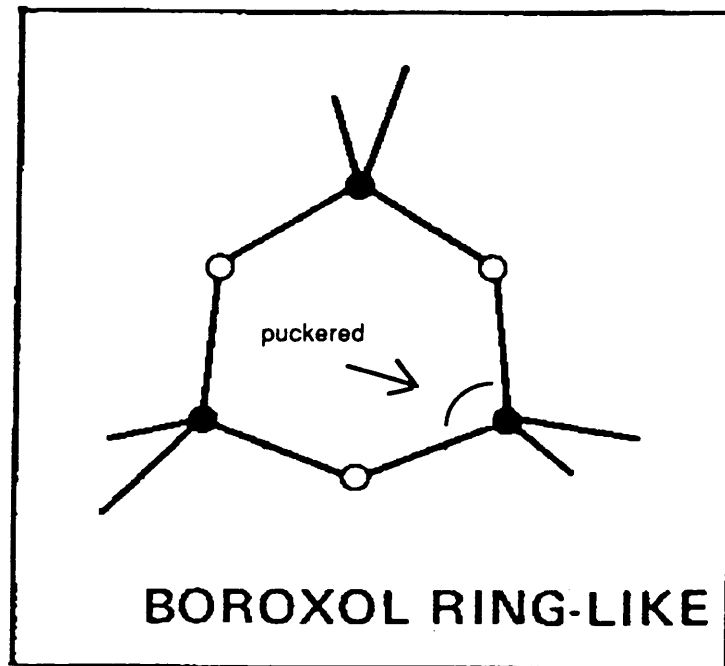
following model, however, serves as a useful aid in interpreting the geochemical trends associated with hydration. The adsorption of water onto a glass surface is a precursor to hydration of that glass, and is followed by diffusion of water along paths of structural weakness. In this study, this concept is important because secondary hydration begins with surface attack followed by diffusion inward towards the center of an obsidian core. Much of the work which supports this type of hydration model has been done using Neutron Magnetic Resonance and Raman spectroscopy. Tossel (1991) used solid state ^{29}Si and ^{17}O Neutron Magnetic Resonance (NMR) to determine structural defects on the surface of amorphous silica. The defects are important because they are hydroxyl bonding sites. The conclusions made from this study were that 3, 4, and 5 coordinated Si can exist in amorphous substances. Comparisons of bridging oxygens in $(\text{SiH}_3)_2\text{O}$ (at 1200°C) and $(\text{BH}_2)_2\text{O}$ (at 1320°C) support the use of a 3-member boroxyl ring as a model to explain intermediate range order in glass. This structure has also been used to explain defects detected by Raman spectroscopy (Figure 4). The distortion of the bond angle between Si and O was termed the "pucker angle" (Galeener, 1983), and is accompanied by a change in bond energy which is detected as a strain defect. Raman spectra shows that the O-Si-O bond angle is puckered from 109.50° to 103° (Brinker et al., 1990). The puckered silica tetrahedra are sites where H^+ attaches to O. The puckering and the hydrogen bonding both occur at the transition temperature between a supercooled liquid and a glass (Figure 1) and increase in abundance with higher temperatures. Metastable Si-O-Si bonds can be promoted by fast rates of condensation of water and commonly occur in

altered obsidians, pods, and stringers of felsite. This may be important to explain the rapid hydration associated with fumarolic activity. Porosity ("internal surface content") may also promote hydration related to these defects (Galeener, 1983). This hydration occurs at sites strained at the time of quenching, with intermediate range order resulting as the consequence of the change in bond angles.

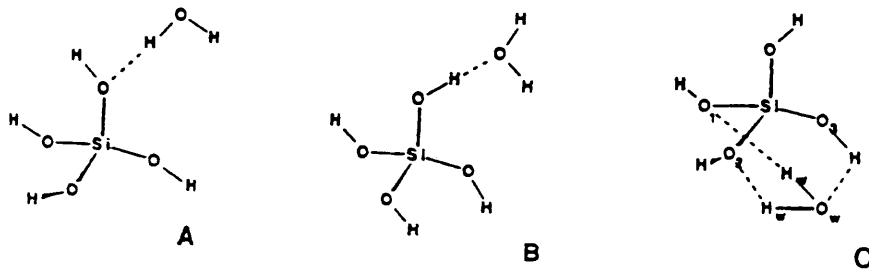
1.6 Previous Studies

1.6.1 Geochemistry The first research which specifically discussed the process of hydration of volcanic glasses was a paper by Ross and Smith (1955). They make reference to work done by Shepherd (1938) which recognized different volatile concentrations for obsidian and perlite. Ross and Smith showed that the water content of glass samples, determined by loss on ignition, is related to the refractive index of the glass. They suggested that perlite was formed by secondary hydration of obsidian.

The above study led the way for research by Friedman and Smith (1958) which determined the deuterium-hydrogen concentrations of water in silicic volcanic glasses (relative to Lake Michigan water). They compared the results to modern meteoric water composition. The perlite samples (collected from flows and domes in the western United States, Iceland, and New Zealand) were found to have deuterium concentrations approximately 4% below that of the meteoric water in the area where they were formed and show no relationship to remnant obsidian nodules within the perlite.



a.) Intermediate range order tetrahedral network. The filled circles represent silicon, and the open circles represent oxygen. The puckered angle is the bonding angle between Si and O. (Modified after Galeener, 1983).



b.) Schematic bond configurations between Si, O, and H. In A, H_2O is a H^+ bond donor, and in B, H_2O is a single H^+ acceptor. The ring shown in C, was computer simulated to predict a combination of bond donor and acceptor configurations. (Taken from Garofalini, 1990).

Figure 4. Tetrahedral Network Configurations

Friedman and Smith (1960) did research which described the geochemical relationship between hydration of obsidian and climatic/temporal controls. This work included microscopy which measured the thickness of hydration rims in obsidian. The data was plotted as a square against ages determined from radiocarbon geochronological estimates, tree-ring dates, or historic information. This procedure is currently used to assign an age to obsidian artifacts.

Meighan (1970) critiqued Friedman's hydration equation that was expressed as,

$$x^2 = kt,$$

where x is the thickness of hydration selvage, k is a constant, and t is time. The importance of temperature was recognized by comparing hydration selvages from 3 different areas. Meighan (1970) also suggested that variations in glass composition may have an effect upon the rate of hydration.

Marshall (1961) discussed the historical development of research related to hydration and devitrification, beginning with Parkinson (in Bonney and Parkinson, 1903). Marshall suggested that hydration was controlled by the rate of diffusion by water throughout the glass along hydration fronts, and was the precursor of devitrification. His treatment was both thermodynamic (in terms of free energy) and kinetic with respect to reaction rates associated with devitrification. Activation energies were used to calculate hypothetical devitrification rates. Strain birefringence was included as evidence of incipient crystallization of crystallites in hydration layers along arcuate fractures in the glass. He measured the thickness of devitrification rinds along surfaces and derived a

trend which suggested that devitrification rates are on the order of 4 or 5 μm in 100 million years. Rare samples of older, well preserved glass gave devitrification rates of 2 μm or 3 μm per 100 million years.

A later study by Noble (1968) attributed the development of fractures in quenched glasses to stress corrosion. This process is believed to be responsible for the development of surfaces which grow in response to crystallographic defects associated with polymerization of hydroxylated sites. Nucleation sites develop on these surfaces and are characterized by primary crystals or strain birefringence which may define the foci of these defects. Subsequent secondary hydration may commence along fractures originating at these sites.

Because the study of alteration gives information on the mobility of ions in glass, it is important to review these studies. Lipman (1965) recognizes 4 stages of alteration:

- 1.) Primary crystallization.
- 2.) Hydration.
- 3.) Secondary devitrification.
- 4.) Leaching.

In Lipman's classification, primary devitrification is encompassed by the term primary crystallization. As Lipman points out, primary devitrification incorporates the transition from liquidus to solidus (vitreous stage) and subsequent vapor phase crystallization which

characteristically occurs in ash flow tuffs. In lava flows, crystallization is at or above the solidus. To clarify the distinction between temperature regimes, primary crystallization is grouped with primary devitrification in contrast to secondary devitrification which occurs at temperatures well below the solidus boundary (at temperatures not exceeding 200°C).

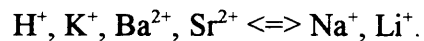
Lipman (1965) compared the chemical composition of hydrated and non-hydrated comagmatic glass samples, and found an increase in Al_2O_3 and K_2O and a decrease in SiO_2 and Na_2O in the hydrated samples. He interpreted these changes as being the result of ground water leaching. Textural variations were interpreted to have an influence on the rate of devitrification and leaching. In particular, rates may have been enhanced by highly permeable units such as vesicular, poorly consolidated tuffs or perlite breccias. In Lipman's study, the alumina increase is interpreted to be residual, while sodium and silica are being leached out. Potassium may increase as a function of ionic exchange, as it substitutes for sodium during leaching. It is also possible that potassium enrichment occurs as a function of potassium metasomatism during devitrification.

In another study, Lipman et al. (1969) show that the oxidation of ferrous iron to the ferric state accompanies hydration in calc-alkalic rhyolites, but not in peralkaline (molecular alkalis > alumina) lavas. This oxidation is attributed to secondary devitrification rather than modification by ground water leaching, as suggested by Noble (1965b) in a study of peralkaline rocks.

Further work supporting Lipman's observations was done by Ewart (1971) on rhyolitic glasses from the Taupo Region of New Zealand. In this study, it was shown that

Na₂O and SiO₂ concentrations are elevated and K₂O, MgO, and MnO are low in secondary spherulites relative to the glassy groundmass. The Na/K content in spherulites is initially low and decreases with the degree of devitrification. The K content of the glassy groundmass increases with progressive devitrification.

Zielinski et al. (1977) characterized Li, Sr, Ba, REE, and halogens concentrations in obsidian and coexisting perlite and felsite. Perlites in their study showed increases in Sr, variable concentrations of Ba, and a decrease in Li relative to obsidian. The geochemical dispersion of alkalis and alkaline earth elements interpreted from the data give the following exchange equation,

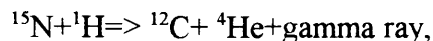


The inferred and measured tendency of this exchange equation is to the left during hydration.

Jezek and Noble (1978), in a microprobe study of hydrated glasses from southern Nevada (including a sample from Delamar), showed that little ion exchange and only slight loss in Na₂O occurred in massive perlite. Along fracture surfaces, small to significantly higher concentrations of water, elevated K₂O, slightly higher MgO, and a depletion of Na₂O were detected. The elevated concentrations were interpreted to represent hydration by diffusion along a surface composed of a "gel-like glass". This structurally altered surface was modified by high ion exchange rates associated with the diffusion of water along a hydration front.

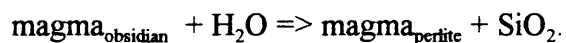
Laursen and Lanford (1978) used nuclear magnetic resonance in a hydrogen

profiling reaction to analyze natural glasses.. The resonance measured the H⁺ concentration from the reaction,



as a function of depth. The assumption made using this technique is that the thickness of the hydration rind is proportional to the square of the time of exposure. This relationship is supported by the Doremus model which postulates that the interaction between alkali and hydronium ions to form hydration layers occurs through ionic interdiffusion.

Marakushev and Yakovleva (1980) concluded from chemical analyses of several dacitic Armenian glasses that oxidation of Fe⁺² in red versus brown and black glasses originating from the same magma chamber reflects differing porosities that control the degree of oxidation. Their study draws primarily upon hypothetical petrologic reactions to show that the waters of hydration are primary rather than secondary. No data is presented to support this hypothesis, and the data which is reviewed is interpreted out of context in which it was given. The conclusion is based upon the reaction,



The authors treat devitrification as a secondary process, which reflects variable chemistry, but describe perlite chemistry as being relatively homogeneous.

Eichelberger and Westrich (1981) analyzed samples from Medicine Lake Highlands, the Inyo Domes, and Crater Lake. Data analysis was done using thermal gravimetric analysis (TGA) which measures volatile contents driven off in response to the application of heat. The evolution of the largest volume of water from tephra-pumice

occurs at temperatures below 400°C. Most of the water from obsidian, in contrast, is liberated at temperatures less than 700°C. The waters evolved from flow-pumice and flow-obsidian show the same relative relationship, but are characterized by significantly smaller water losses at lower temperatures. The study concludes that the water contents of tephra (as measured by TGA analysis) range from 0.5-1.0 wt.% H₂O, and represent a density controlled stratification above the magma chamber which contains 0.1 - 0.2 wt.% H₂O.

Taylor et al. (1983) report water contents of obsidian and pumice in tephra and flows from Medicine Lake (Little Glass Mountain and Glass Mountain), Mammoth Lakes, and Newberry Crater. Several values reported for samples from Little Glass Mountain range from 1.04 - 3.12% H₂O, well above the range expected in fresh obsidian samples (0.1 - 0.3%), although adsorption of atmospheric moisture upon sample preparation or calibration errors may explain these anomalous values.

Friedman and Long (1984) summarized the petrochemistry and hydration of natural glasses, ranging from basaltic through rhyolitic compositions. Hot, non-viscous basaltic flows show slow hydration rates as compared to viscous, highly polymerized rhyolitic glasses. In other words, as the concentration of silica increases, so does the rate of hydration. The rate of hydration was also found to decrease with increasing concentrations of CaO and MgO. Experimentally measured rates of crystal growth as a function of temperature and pressure put useful constraints upon devitrification. These data show that glasses are metastable with respect to time and the rate of devitrification is

controlled by the activation energy of viscosity, which increases following emplacement. Another important factor is the release of volatiles within the glass upon crystallization. Anhydrous mineral growth during devitrication is accompanied by the outward diffusion of a selvage of water surrounding the crystal. The water diffuses away from the growing crystal during vapor phase crystallization. Increasing the water of crystallization lowers the activation energy and promotes further devitrification.

Nickel (1987) analyzed Oligocene glass samples from a topaz rhyolite intrusive from Ruby Mountain, Colorado. Perlite and pitchstone samples, typically severely altered to a mixture of clay and glass, were studied with an emphasis on geochemical characterization. As described by Nickel, the Ruby Mountain samples are "primitive" in contrast to other topaz rhyolites.

Elements depleted in the Ruby Mountain samples, but normally high in topaz rhyolites, include Rb, Cs, U, Th, and F. All of these elements are highly mobile and their concentrations may represent leaching during hydration or devitrification. Other elements leached from the glass during hydration are H^+ , Na^+ , and K^+ . Residual increases were noted for the following elements, Mg, Ca, Sr (?), Ba, Al, and F. Fe, Co, Cu, Hf, Ta, La, and Ce were liberated during leaching of the glass. Petrologically, the felsite and obsidian samples from Ruby Mountain are metaluminous (molecular concentration of $Al_2O_3 > Na_2O + K_2O$, but $< Na_2O + K_2O + CaO$), in contrast to the peraluminous (molecular concentration of $Al_2O_3 > Na_2O + K_2O + CaO$) perlite, pitchstone, and pyroclastic rocks. The conclusion drawn from these observations is that the residual increase in alumina and

the loss of alkalis are responsible for the discrepancy in classifications.

Macdonald et al. (1992) presented geochemical data on a large suite of rhyolite glass samples, grouped by tectonomagmatic environments, and categorized with respect to magmatic differentiation processes. Trace element discrimination plots were used to identify trends within groups, and systematic geochemical variation diagrams were used to display genetic trends within groups. The tectonomagmatic groups are listed below,

Group	Occurrence	Tectonic Setting
I.)	Primitive island arcs	Subduction
II.)	Mature island arcs	Subduction
III.)	Continental margins	Subduction
IV.)	Continental interiors	Extension
V.)	Oceanic Extensional zones	Extension

This classification is particularly useful for identifying geochemical trends in glasses.

1.6.2 Spectroscopy The field of infrared spectroscopy is relatively new as compared with traditional chemical analyses, x-ray diffraction, and emission spectrographic analyses. The behavior of light, in simplest terms, is best described by the equation ,

$$c = \lambda \nu,$$

where c is the velocity of light, λ is the wavelength, and ν is the frequency. Figure 3 illustrates the relative position of the infrared spectra with respect to wavelength, which increases to the right.

Among the earliest studies of the spectral signature of hydrated volcanic glasses, were those of Keller and Pickett (1954). They used transmission spectroscopy, and showed absorptions at 2.8 and 6.1 μm .

As a precursor to the use of remote sensing in mineral exploration, Hunt and Salisbury (1970) did pioneering research in reflectance spectroscopy. Their paper describes the spectral absorption of OH^- stretching at 2.2 - 2.3 μm produced by lattice vibrational motion.

The fundamentals for these vibrational frequencies are located in the mid- and far-infrared (IR), and the overtone and combination tone features show up in the near-IR and visible ranges (Figure 5). Overtones are produced when two or more quanta excite a fundamental frequency. The resulting frequency produced has a higher frequency than the fundamental, with a decreased band intensity. Combinations arise from constructive and destructive interference of two or more fundamentals. Strictly harmonic motions are forbidden, although anharmonic motions are permissible. Overtones and combinations are produced by materials with high fundamental frequencies.

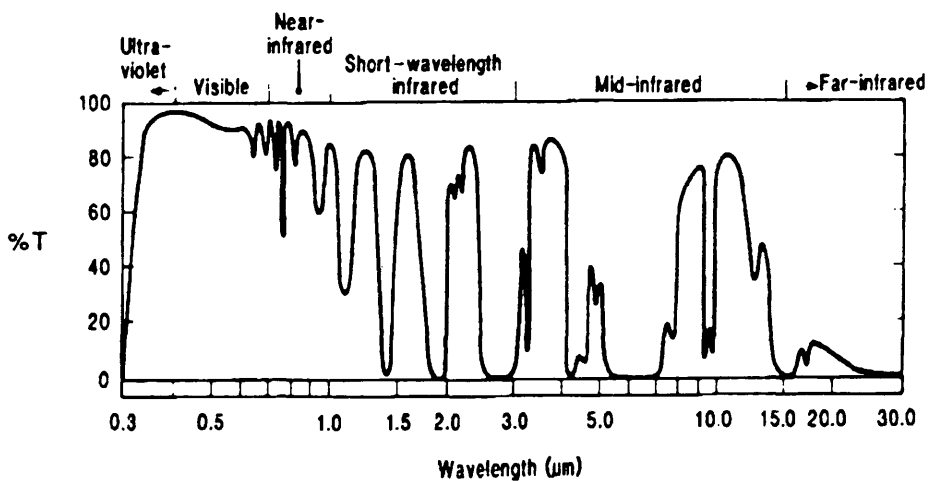


Figure 5. Subdivisions of the Infrared Spectrum

Absorption spectrum of the atmosphere with spectral regions labeled at the top of the plot. The wavelength is measured in microns (μm) and is shown at the bottom of the plot. Absorption is measured in % transmission (%T). (Taken from Goetz and Rowan, 1981).

Aines and Rossman (1984) discuss the various vibrational motions associated with molecular water. The first type of motion described is the symmetric stretch, where the hydrogen atoms are drawn inward toward the oxygen atom (Figure 6). In the asymmetric stretch, one hydrogen atom vibrates toward the oxygen atom and the other vibrates away from it. A fluctuation in the bonding angle is labeled a bend. Lattice vibrations are produced by anions such as OH^- , with fundamentals in the mid- and far-IR and overtones and combination tones showing up in the near-IR and visible range.

In the near-IR, molecular water displays sharp, easily detectable absorption

features. The fundamental vibrational modes produced in ice are generally used to estimate the fundamentals for water dispersed throughout solids. These are listed below:

- 1.) The symmetric OH⁻ stretch, at 3.105 μm (ν_1).
- 2.) The H-O-H bend at 6.06 μm (ν_2).
- 3.) The asymmetric OH⁻ stretch, at 2.941 μm (ν_3).

In rocks and minerals, diagnostic bands occur at 1.4 μm (from $\nu_3 + \nu_3$, OH⁻ + OH⁻) and at 1.9 μm (from $\nu_2 + \nu_3$, H-O-H + OH⁻ and OH⁻). The presence of the 1.4 μm band (molecular water absorption with absorption produced by either dissociation of molecular water, or hydroxyl vibrations) in the absence of the 1.9 μm band (molecular water absorption) establishes the existence of OH groups not related to the dissociation of molecular water.

In some substances, an OH⁻ stretching mode can combine with a vibrational mode to produce a band in the 2.2 μm region. This band can be strongly directional, particularly when Al substitutes for Si, widening the band at 2.2 μm with increasing Al/Si. This means that the 2.2 μm band may be dominated by this substitution in these structural network-forming sites.

In this study the 1.9 μm molecular water band, and the 2.2 μm hydroxyl water band were chosen as the optimal bands because both are found in the short-wavelength IR region. The 1.9 μm band is produced by constructive interference of the 2.8 μm H₂O

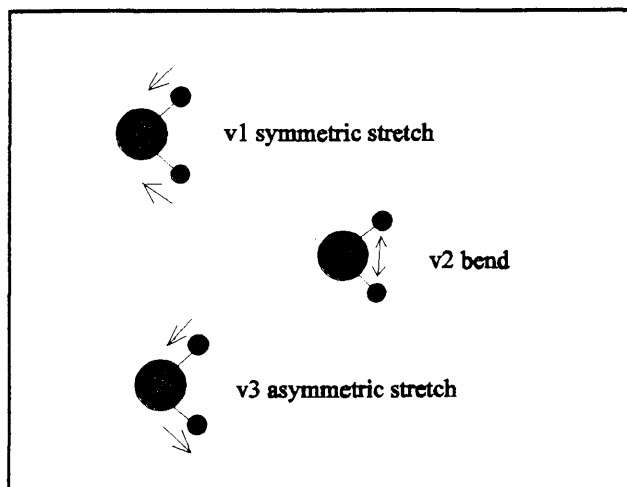


Figure 6. Vibrational motions of H₂O

Three vibrational motions in H₂O are shown in this sketch. The large circles represent oxygen, and the small circles represent hydrogen.

stretch combined with the H₂O bend at 6.1 μm (Clark, pers. comm., 1994), and the 2.2 μm band is a combination of the OH⁻ stretch at 2.8 μm with the Si-OH, Al-OH bends at 10 and 11.1 μm (Table I). The instrumentation effectively measures IR transmission in the short-, mid- or far-IR, and the amount of sample needed varies according to the strength of the band. The 1.9 μm band and the 2.2 μm band both require the same amount of sample, and this expedited sample preparation and analysis. It was not possible to detect the 1.4 μm band due to adjustment problems with the instrumentation. The reliability of measurements using the 2.8 μm band is compromised by the intensity of the signal.

Table I - Band Assignments

Band Assignment	Peak	Geometry/mode	Reference
OH ⁻ , H ₂ O - stretch	2.82 um	Asymmetrical/ symmetrical fundamental.	Nakamoto (1978), Scholze (1959), Paterson (1982)
OH ⁻ stretch, - H ₂ O stretch	1.41 - 1.47 um	1st overtone of 2.8 um fundamental	Bartholomew et al. (1980)
H ₂ O - bending	6.13 um	Symmetrical fundamental	Nakamoto (1978)
H ₂ O ?	1.79 um	Combination	Newman et al. (1986)
H ₂ O bend/stretch	1.92 um	Combination 6.1 bend + 2.82 um stretch	Scholze (1960), Bartholomew et al. (1980)
SiOH Al-OH	2.22 um	Combination 2.82+10+11.1um	Scholze (1966) Stolper (1982)
H-bonded SiOH, H ₂ O, X-OH, and dissolved H ₂ O	2.50 um	Combination, assignment uncertain	Wu (1980) Stolper (1982) Acocella et al. (1984)

Chapter 2. METHODS

2.1 Transmission Samples

The samples used in this study are listed in Table II. These were taken from silicic volcanic domes and dome-flow complexes, located worldwide, and were comprised of primary and secondary volcanic glass.

2.2 Transmission Sample Preparation

Sample preparation was done at the Isotope Geology Lab at the U.S.G.S. Federal Center, in Denver Colorado. The transmission samples were crushed, sieved, dried, weighed, mixed with potassium bromide, and compressed into pellets. It was necessary to use powdered samples for the analysis of perlite because perlite is characterized by microscopically intricate fractures which make it difficult, if not impossible, to cut slabs to the thicknesses required to measure absorption in the short wavelength and middle-range infrared.

This procedure began with crushing the sample with a mortar and pestle to a fine powder. This powder was then sieved to a mesh fraction of -80+270 (-250+90um), dried in an oven for 15 minutes at 110⁰ C, removed, and cooled in a desiccator before weighing.

Table II Sample Locations

Sample Name	Sample Location	Latitude/Longitude	Source
Arroyo Hondo Obsidian	Sandoval County, New Mexico	35-35-N/106-40-W	Irving Friedman
Arroyo Hondo Perlite	Sandoval County, New Mexico	35-35-N/106-40-W	Irving Friedman
Askja Obsidian	Iceland	65-2-N/16-42-W	Irving Friedman
Bald Mountain Obsidian/Perlite	Chaffee, Colorado	38-47.43-N/106-1.72-W	James Piper
Bald Mountain Perlite	Chaffee, Colorado	38-47.43-N/106-1.72-W	James Piper
Bearhead Pitchstone	Sandoval County, New Mexico	35-45-N/106-30-W	Irving Friedman
Big Pine Obsidian	Inyo County, California	37-3.38-N/118-17.87-W	Irving Friedman
Big Pine Perlite	Inyo County, California	37-3.38-N/118-17.87-W	Irving Friedman
Big Glass Mountain Pumice	Modoc County, California	41-37.43-N/121-27.66-W	Irving Friedman
Big Glass Mtn. Obsidian	Modoc County, California	41-37.43-N/121-27.66-W	Irving Friedman
Black Springs 87-10 44-54' Perlite	Millard County, Utah	38-43.51-N/112-49.48-W	James Piper
Black Springs Obsidian	Millard County, Utah	38-43.51-N/112-49.48-W	Irving Friedman
Canovas Obsidian	Sandoval County, New Mexico	35-41.76-N/106-34.08-W	Irving Friedman
Canovas Perlite	Sandoval County, New Mexico	35-41.76-N/106-34.08-W	Irving Friedman
Coso Obsidian	Inyo County, California	36-5-N/117-47-W	Christopher Stevenson
Cudahy Mahogany Obsidian	Millard County, Utah	38-43.51-N/112-49.48-W	James Piper
Cudahy Perlite	Millard County, Utah	38-43.51-N/112-49.48-W	James Piper
Delamar Perlite	Lincoln County, Nevada	37-20-N/114-30-W	Robert Scott
Frazier Canyon Obsidian	Sandoval County, New Mexico	35-45-N/106-30-W	Irving Friedman
Japan Dacite	Location Unknown	Location Unknown	Irving Friedman
Macusanite	Macusani, Peru	70-27-W /14-4-S	Irving Friedman
Medicine Lk. Hoffman Obsidian	Modoc County, California	41-37.43-N/121-27.66-W	Irving Friedman
Mt. Floyd Smith Tank Obsidian	Coconino County, Arizona	35-45-N/113-W	David Neally
Mt. Floyd York Perlite	Coconino County, Arizona	35-45-N/113-W	David Neally
No Agua Grefco HW Obsidian	Taos County, California	36-45.68-N/105-56.97-W	Irving Friedman
No Agua Grefco Perlite 35093	Taos County, New Mexico	36-45.68-N/105-56.97-W	Irving Friedman
No Agua Obsidian 35125	Taos County, New Mexico	36-45.68-N/105-56.97-W	Irving Friedman
No Agua Perlite 35125	Taos County, New Mexico	36-45.68-N/105-56.97-W	Irving Friedman
No Agua Perlite 351216	Taos County, New Mexico	36-45.68-N/105-56.97-W	Irving Friedman
Olancha2 Obsidian	Inyo County, California	36-20.54-N/117-50.61-W	Irving Friedman
Olancha2 Perlite	Inyo County, California	36-20.54-N/117-50.61-W	Irving Friedman
Panum Grey Glass	Mono County, California	37-55.88-N/119-2.47-W	Irving Friedman
Panum Obsidian	Mono County, California	37-55.88-N/119-2.47-W	Irving Friedman
Peralta Obsidian	Sandoval County, New Mexico	35-25-N/106-30-W	Irving Friedman
Peralta Perlite	Sandoval County, New Mexico	35-25-N/106-30-W	Irving Friedman
Priest Mtn. Obsidian	Iceland	63-45.31-N/20-42-W	Irving Friedman
Priest Mountain Perlite	Iceland	63-45.31-N/20-42-W	Irving Friedman
Ruby Mountain Pitchstone	Chaffee, Colorado	38-47.43-N/106-1.72-W	James Piper
Superior Obsidian	Cochise County, Arizona	31-45-N/109-30-W	Irving Friedman
Superior Perlite	Cochise County, Arizona	31-45-N/109-30-W	Irving Friedman
Thomas Obsidian	Juab County, Utah	39-45-N/113-W	Irving Friedman
Xalazaquilla HW Obsidian	Puebla, Mexico	19-14-N/97-26-W	Irving Friedman
Xalazaquilla Obsidian	Puebla, Mexico	19-14-N/97-26-W	Irving Friedman
Xalazaquilla Perlite	Puebla, Mexico	19-14-N/97-26-W	Irving Friedman
OTHER GLASSES			
Libyan Glass	Location Unknown	Location Unknown	Irving Friedman
Opal Beaver Co. UT.	Beaver County, Utah	Location Unknown	Colorado School of Mines

30 mg of the sample was mixed with a 270 mg sample of Baker's optical grade KBr. This mixture of glass and KBr was placed into a Wiggle-bug capsule and homogenized by vigorous vibration for 2-3 minutes. The homogenized sample was then poured into a die and compressed into a pellet approximately 1cm in diameter and 1mm in thickness. A 300 mg blank of homogeneous KBr was also prepared and used to measure background absorption. This sample allows the calculation of the actual transmission of the samples, by subtracting the absorption by the KBr.

The main problem with analyzing glasses that have been ground to fine powders (-80+250 mesh) is that atmospheric water adsorption occurs at an extremely fast rate and may interfere with accurate measurements if precautions are not taken to minimize the exposure time. To minimize the degree of contamination from atmospheric water adsorption, the duration of atmospheric exposure was minimized by storing the pellets in a desiccator.

At the onset of this study, acetone was used to wash the samples in an attempt to remove water adsorbed onto the surfaces of grains. It was found that this procedure resulted in a residue of acetone (CH bands) on the surface of the grains that caused absorption in the 3-4 um region of the spectrum. This contamination interfered with the interpretation of spectral features, including deuterium and silanol bands which characteristically occur within this portion of the spectra. Acetone was accordingly eliminated as a step in the analytical routine.

The first several batches of samples were run using laboratory grade KBr, which is

coarser grained than optical grade and has more impurities. To validate the use of this grade of KBr, a sample of optical grade KBr was compared to a sample of laboratory grade KBr: no significant differences were observed in the 1.9 μ m band. The optical grade KBr was heated 24 hours in an oven at a temperature of 110^o C and cooled in a desiccator prior to weighing.

2.3 Transmission Procedures

The spectral transmission through the pellets was measured using a Nicolet FTIR 740 infrared spectrometer. The procedure used for sample analysis is presented below.

- 1.) A KBr blank was positioned in the spectrometer using a sample holder. A magnetic card with an opening approximately 800 μ m in diameter was used to hold the sample in place.
- 2.) Laser light was transmitted through the sample and its intensity was optimized to a value at the upper end of the instrument transmitted scale. The Fourier transform of the transmitted light was graphically displayed.
- 3.) The same process was repeated for each sample. The data was then transferred to a program written to analyze spectral features. This program, SPECPR (Clark, 1993) is written in Fortran for use in a Unix C shell. SPECPR enables the user to quantitatively measure the depths of spectral

absorption bands, and make spectral calculations.

2.4 Transmission Calibration

To calibrate the magnitude of the absorption from powdered samples, high precision water analyses were plotted against the absorption coefficients to derive a linear best-fit solution. The coefficients for slabs of obsidian were then derived using this method to determine the variations between transmission through slabs and grains dispersed throughout a KBr host. The regression statistics for these coefficients were used to calibrate the data and assess the accuracy of the method. The calibrated coefficients were then used to calculate the proportions of hydroxyl to molecular water in the powdered samples.

Chapter 3. DATA

3.1 Geochemical Characterization

The major element compositions of the obsidians are taken from Macdonald et al. (1992), Austin and Barker (1994), Whitson (1982), Friedman (pers. comm., 1994), and David Neally (pers. comm., 1994). These values are reported in wt.% (Table III). Of the thirty-two chemistries selected, twenty-seven of these were reported by Macdonald et al. (1992). The analytical precision for five replicate analyses (in percent) of an obsidian from Pantelleria was reported as: SiO_2 66.5 ± 0.11 (at one standard deviation), Al_2O_3 10.61 ± 0.05 , Fe_2O_3 2.23 ± 0.13 , FeO 6.15 ± 0.07 , MgO 0.15 ± 0.004 , CaO 0.56 ± 0.005 , Na_2O 7.47 ± 0.03 , and K_2O 4.52 ± 0.00 (Macdonald et al., 1992).

A plot of SiO_2 (wt.%) against $\text{Na}_2\text{O} + \text{K}_2\text{O}$ and CaO (Figure 7) shows that the samples in this data set are calcic. $\text{Na}_2\text{O} + \text{K}_2\text{O}$ concentrations are lower for the 4 samples listed below (and follow a subparallel linear trend),

- 1.) Askja obsidian
- 2.) Grefco No Agua HW obsidian
- 3.) No Agua obsidian 35125
- 4.) Priest Mountain obsidian

Table III - Chemistry (wt.%)

Sample Name/Type	% H2O	%SiO2	%Al2O3	%Fe2O3	%FeO	%MgO	%CaO	%Na2O	%K2O	Total %Oxides
Obsidian - Perlite Pairs										
Big Pine Obsidian	0.18	76.65	13.30	0.38	0.34	0.05	0.53	4.55	4.43	100.23
Big Pine Perlite	2.90	74.59	13.03	0.73		0.08	0.60	4.00	4.85	97.89
No Agua Obsidian 35125	0.31	75.50	14.60	0.85		0.10	0.55	3.10	4.20	98.90
No Agua Perlite 35125	2.30	73.60	13.32	0.45	0.22	0.05	0.84	4.06	4.37	96.91
Superior Obsidian	0.23	76.66	12.68	0.35	0.36	0.09	0.48	4.05	4.61	99.28
Superior Perlite	3.40	75.11	12.98	0.60		0.32	0.81	3.96	4.57	98.35
Unpaired Samples										
Askja Obsidian	0.13	72.10	12.77	1.11	2.84	0.73	2.69	4.08	2.30	98.62
Big Glass Mtn. Obsidian	0.09	73.30	13.99	0.41	1.29	0.26	1.23	4.12	4.33	99.02
Black Springs Obsidian	0.38	76.30	13.09	0.29	0.58	0.03	0.78	3.83	4.75	99.65
Canovas Obsidian	0.21	76.40	12.74	0.39	0.30	0.06	0.43	4.31	4.55	99.18
Cudahy Mahogany Obsidian	0.03	75.90	12.96	0.33	0.56	0.02	0.79	3.86	4.71	99.13
Macusanite	0.23	70.67	16.12	1.33	0.41	0.18	2.07	3.30	5.53	99.61
Medicine Lk. Hoffman Obsidian	0.33	73.30	13.99	0.41	1.29	0.26	1.23	4.12	4.33	98.93
Mt. Floyd Smith Tank Obsidian	0.12	76.80	12.80	0.87		0.06	0.44	4.20	4.47	99.64
Mt. Floyd York Perlite	2.13	74.20	12.40	0.91		0.08	0.43	3.80	4.68	96.50
Panum Grey Glass	0.26	76.50	12.51	0.33	0.76	0.02	0.52	3.96	4.59	99.19
Panum Obsidian	0.25	76.50	12.51	0.33	0.76	0.02	0.52	3.96	4.59	99.19
Priest Mtn. Obsidian	0.13	76.73	12.26	0.45	1.15	0.10	1.08	4.29	3.32	99.38
Xalazaquilla Obsidian	0.12	76.71	12.29	0.41	0.81	0.01	0.42	3.87	4.91	99.55
Xalazaquilla Obsidian	0.12	76.71	12.29	0.41	0.81	0.01	0.42	3.87	4.91	99.43
High Water Glasses										
No Agua Grefco HW Obsidian	0.50	74.50	13.30	0.70		0.30	1.30	2.30	4.30	96.70
Olancha2 Obsidian	0.95	75.93	12.73	0.35	0.45	0.05	0.46	4.51	4.24	98.72
Xalazaquilla HW Obsidian	0.98	74.20	14.04	0.09	0.52	0.03	0.48	4.42	4.15	97.93
Other Glasses										
Libyan Glass	0.06	97.58	1.54	0.11	0.23		0.38	0.34		100.24

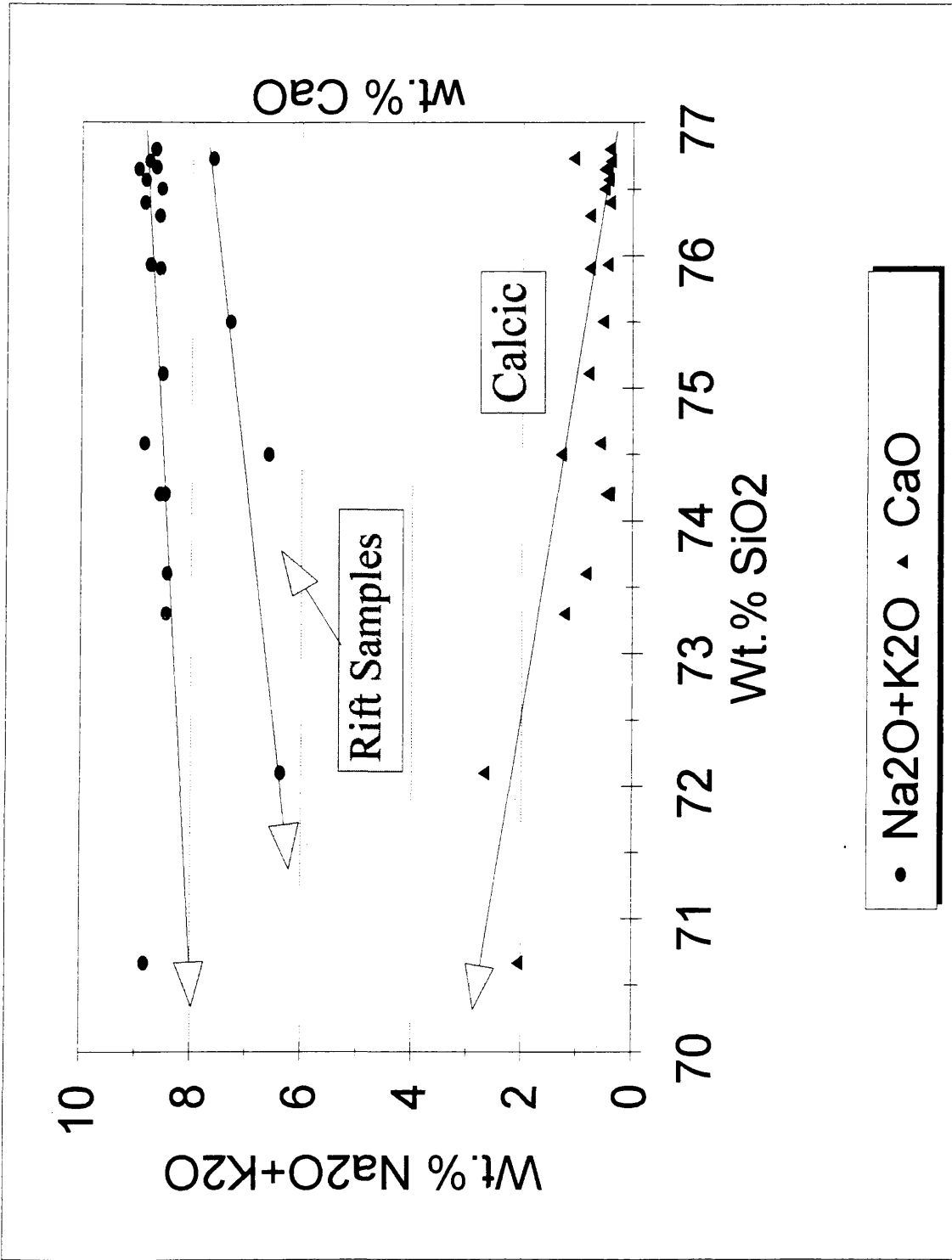


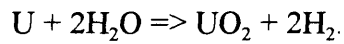
Figure 7. Na₂O + K₂O & CaO versus SiO₂

The two Icelandic samples (Priest Mountain obsidian and Askja obsidian) are from silicic magmas associated with the Mid-Atlantic Ridge (oceanic extensional zone), and the two No Agua samples are spatially associated with the Rio Grande Rift (continental interior, extensional zone).

Manometric combined water concentrations determined by Irving Friedman were also reported in the major element compositions from Macdonald et al. (1992). Combined manometric water concentrations were used to calibrate all of the infrared data. These quantitative determinations are accurate to $\pm 0.05\%$ combined error in weighing the sample and uncertainty in the amount of water present (Friedman and Smith, 1958). The combined error for IR water determinations in this study is comparable to the reported combined error for the manometric water determinations (for discussion of results see section 3.2). The procedure used for manometric water determinations is summarized below:

- 1.) 0.3-10 grams of the sample is weighed to ± 0.01 grams and placed into a platinum crucible capped by a platinum lid.
- 2.) The platinum container is placed into a quartz tube which is evacuated.
- 3.) The sample is preheated to 110°C in a vacuum to remove adsorbed water.
- 4.) The sample is then quickly heated to a temperature of 700°C , followed by a gradual increase in temperature to 1450°C .
- 5.) The evolved water is trapped and condensed with liquid nitrogen.
- 6.) The water is allowed to evaporate, and the vapor is exposed to uranium metal

heated to 600°C to produce the reaction,



H₂ gas is collected and its volume is measured by a manometer.

3.2 Water Analysis

A total of 47 powdered samples, and 7 polished slabs were examined using transmission spectroscopy. The spectral data was collected and mathematically converted into absorbance using Bouguer-Beer's Law,

$$\ln I_0/I = A = \epsilon \rho d c = -\ln T,$$

where:

I_0 = incident radiation

I = emergent radiation

ϵ = molar absorptivity (extinction coefficient) - L/mol*cm

ρ = density - gm/L

d = thickness - cm

c = concentration - weight fraction

A = absorbance - dimensionless

T = transmission - dimensionless.

From this relationship,

$$T = I/I_0 = \epsilon \rho d c,$$

$$A = \ln T = \ln e^{-\epsilon p d c},$$

and

$$A = -\ln T = \epsilon k c,$$

where

$$k = \rho * d.$$

The absorbance was calculated using SPECPR. The depths of the absorbance bands were graphically determined. These values were used to derive the molecular (at 1.9 μm) and hydroxyl (at 2.2 μm) water concentrations of the samples.

The calibration for the KBr pellets was derived from the spectra of 32 samples (Table IV). The amount of glass used in each sample was optimized at 30 mg. The regression statistics for this data set show an R^2 of 0.87, with a slope of 0.02 (Figure 8). There is a wide gap between the obsidian population (0.07-0.98% H_2O) and the perlite population (2.30-3.90% H_2O). The scatter in the perlite samples may reflect sample size (11 perlite samples versus 21 obsidian samples), or changes in the relative band strengths (1.9 μm /2.2 μm) as a function of the changes in $[\text{H}_2\text{O}]/[\text{OH}^-]$.

To establish the optimal calibration for the powdered samples, 7 slabs were polished on each side (Table IV). The regression statistics show an R^2 value of 0.92 (Figure 9), with a slope of 1.01. This plot shows the optimal accuracy for the combination of the 1.9 μm and 2.2 μm bands using the Nicolet.

The total water, molecular and hydroxyl species, for 15 powdered samples was determined subsequently without the aid of manometric data (Table V).

Table IV - Absorbance/Manometric H₂O - Calibration Samples

Powdered Samples	File #	1.9um band	2.2um band	1.9+2.2um band	Wt.% Man. H2O
Arroyo Hondo Obsidian	4897	0.0099	0.0038	0.0137	0.29
Arroyo Hondo Perlite	4909	0.0441	0.0080	0.0521	2.70
Askja Volcanic Glass	4921	0.0000	0.0018	0.0018	0.15
Bearhead Pitchstone	4933	0.0391	0.0112	0.0503	3.86
Big Pine Perlite	4981	0.0406	0.0077	0.0483	2.90
Big Pine Obsidian	4969	0.0026	0.0058	0.0084	0.18
Big Glass Mountain Obsidian	4945	0.0000	0.0016	0.0016	0.10
Big Glass Mountain Pumice	4957	0.0000	0.0024	0.0024	0.26
Canovas Obsidian	5005	0.0035	0.0066	0.0101	0.21
Canovas Perlite	5029	0.0472	0.0072	0.0544	2.90
Japan Dacite	5065	0.0000	0.0015	0.0015	0.11
Macusanite Glass	5101	0.0010	0.0058	0.0068	0.23
Medicine Lk. Hoffman Obsidian	5125	0.0023	0.0031	0.0054	0.33
No Agua Obsidian 35125	5161	0.0028	0.0096	0.0124	0.31
No Agua Perlite 35125	5185	0.0377	0.0063	0.0440	2.30
No Agua Grefco HW Obsidian	5425	0.0041	0.0098	0.0139	0.50
No Agua Grefco Perlite 35093	5053	0.0408	0.0074	0.0482	3.00
No Agua Perlite 351216	5173	0.0375	0.0048	0.0423	3.00
Olanca2 Obsidian	5221	0.0093	0.0123	0.0216	0.95
Olanca2 Perlite	5233	0.0563	0.0144	0.0707	3.10
Panum Grey Glass	5245	0.0000	0.0053	0.0053	0.31
Panum Obsidian	5257	0.0019	0.0093	0.0112	0.25
Priest Mountain Obsidian	5269	0.0000	0.0032	0.0032	0.17
Priest Mountain Perlite	5281	0.0369	0.0083	0.0452	3.90
Superior Obsidian	5293	0.0012	0.0047	0.0059	0.23
Superior Perlite	5305	0.0666	0.0162	0.0828	3.40
Thomas Obsidian	5317	0.0000	0.0012	0.0012	0.24
Xalazaquilla Obsidian	5389	0.0019	0.0091	0.0110	0.12
Xalazaquilla Obsidian	5377	0.0015	0.0091	0.0106	0.12
Xalazaquilla Perlite	5401	0.0388	0.0072	0.0460	3.10
Xalazaquilla HW Obsidian	5353	0.0055	0.0227	0.0282	0.98
Libyan Desert Glass	5077	0.0000	0.0017	0.0017	0.07
Polished Slabs	File #	1.9um band	2.2um band	1.9/1.9+2.2um	Wt.% Man. H2O
Budweiss Tektite	5413	0.0000	0.0000	0.0000	0.00
Libyan Desert Glass	5089	0.0000	0.0810	0.0000	0.07
No Agua 351216 Obsidian	5209	0.0382	0.2453	0.1347	0.13
Macusanite	5113	0.0244	0.1583	0.1337	0.23
No Agua 35125 Obsidian	5197	0.0033	0.1396	0.0229	0.31
No Agua Grefco HW Obsidian	5041	0.0361	0.2000	0.1529	0.50
Xalazaquilla HW Obsidian	5365	0.3757	0.7305	0.3396	0.98

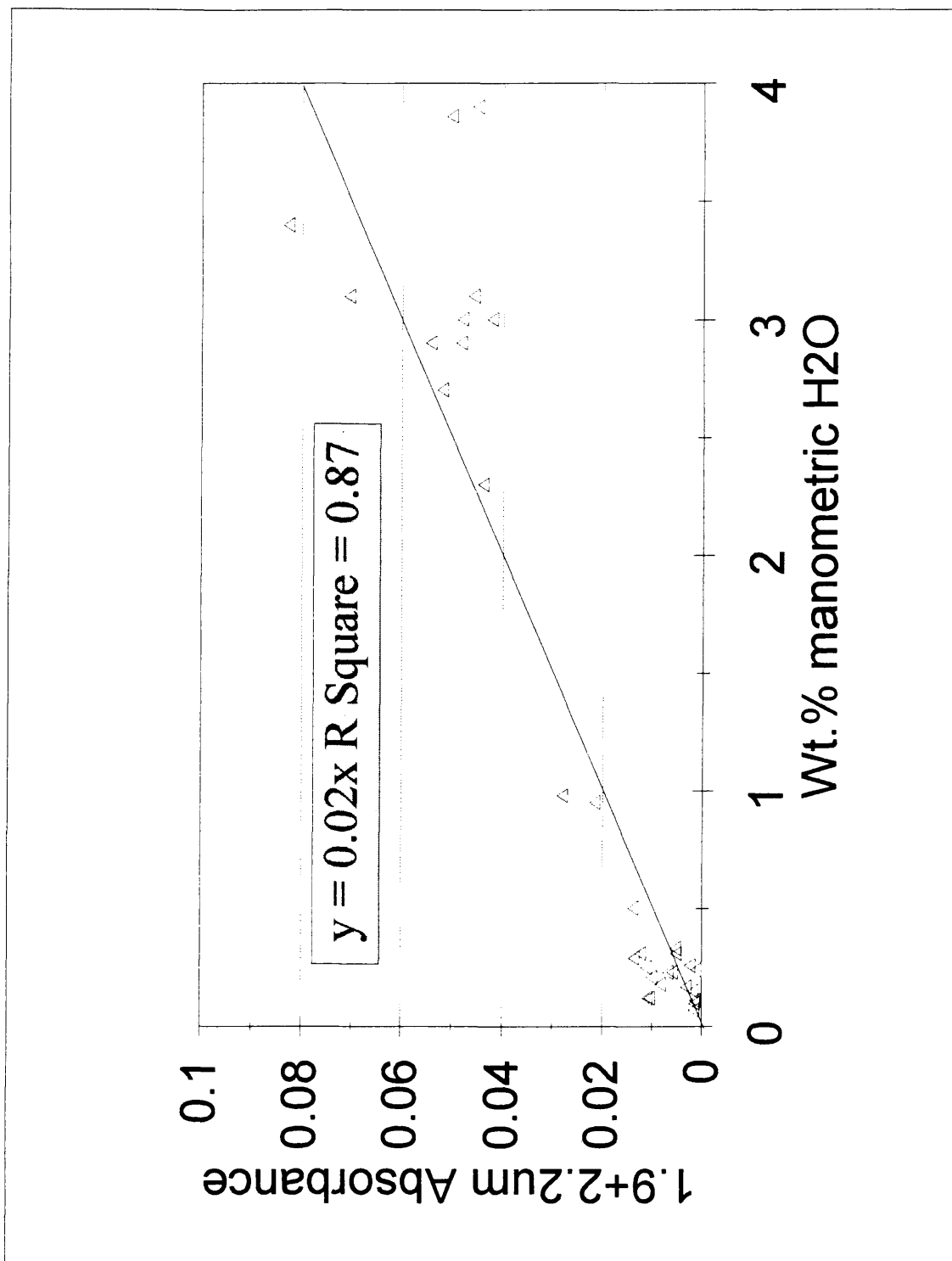


Figure 8. Absorbance versus Manometric H₂O - KBr Pellets

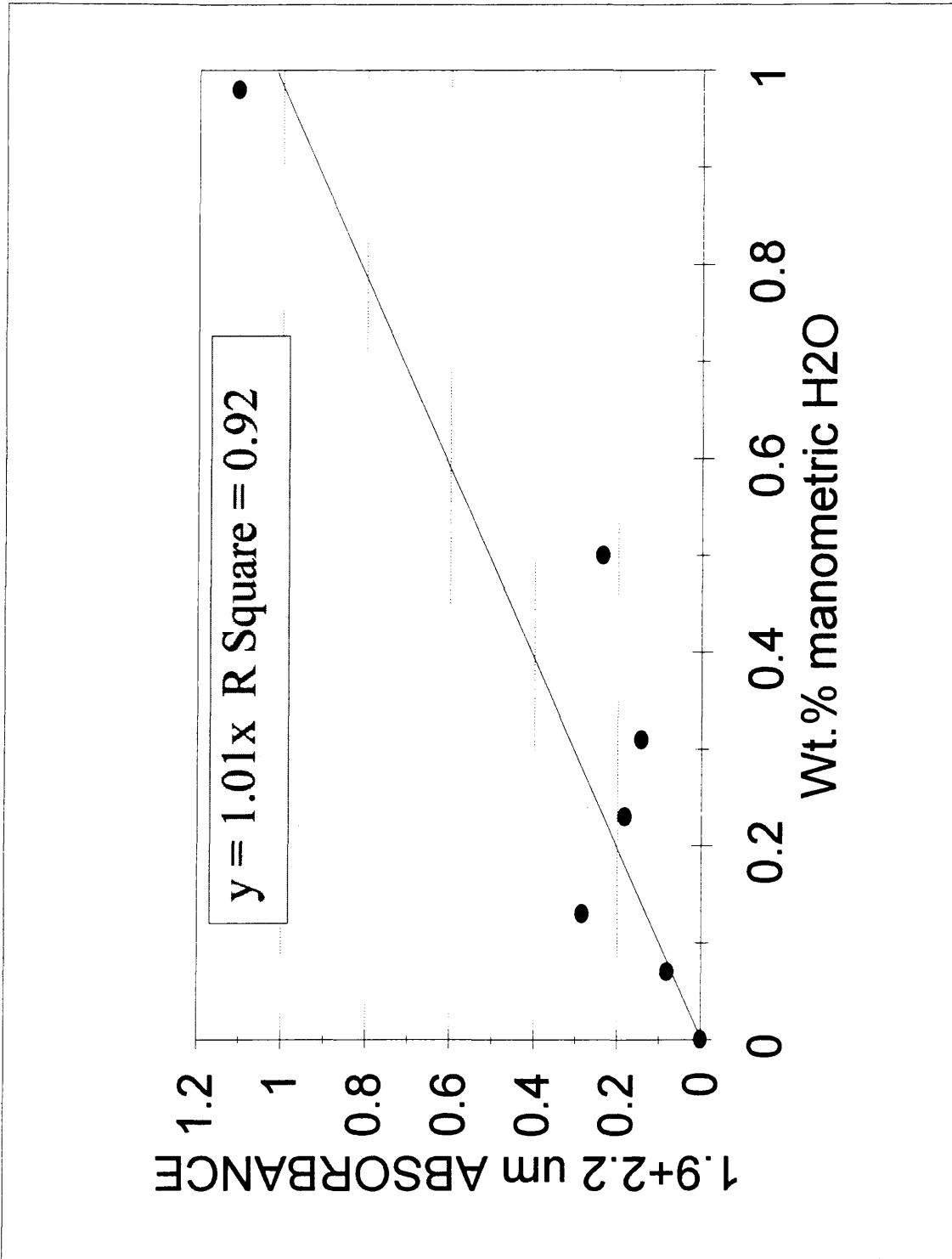


Figure 9. Absorbance versus Manometric H₂O - Slabs

Table V - Absorbance/Manometric H₂O - Unknowns

Sample Name	File#	1.9um band	2.2um band	1.9+2.2um band
Bald Mountain Obsidian	5437	0.0325	0.0056	0.0381
Bald Mountain Perlite	5449	0.0526	0.0087	0.0613
Black Springs Obsidian	5461	0.0029	0.0047	0.0076
Black Springs 87-10 44-54' Perlite	5473	0.0279	0.0026	0.0305
Coso Obsidian	5485	0.0088	0.0149	0.0236
Cudahy Perlite	5497	0.0435	0.0071	0.0507
Cudahy Mahogany Obsidian	5509	0.0000	0.0007	0.0007
Delamar Perlite	5521	0.0327	0.0073	0.0400
Frazier Canyon Obsidian	5533	0.0495	0.0127	0.0623
Mount Floyd Smith Tank Obsidian	5545	0.0000	0.0023	0.0023
Mount Floyd York Perlite	5557	0.0361	0.0066	0.0427
Opal Beaver County Utah	5569	0.0378	0.0117	0.0496
Peralta Perlite	5581	0.0407	0.0083	0.0490
Peralta Obsidian	5593	0.0055	0.0034	0.0088
Ruby Mountain Pitchstone	5605	0.0428	0.0088	0.0516

The variation of the absorbance (the residual) due to scatter in this data set is assumed to be comparable to the degree of scatter in calibration samples. By making this assumption it is inferred that the error (degree of scatter) introduced is either a function of the inhomogeneity of sample grain dispersion throughout the KBr pellet, instrumental error, or a combination of both. The regression established by the 32 calibration samples was used to correct for scatter in these samples by adjusting the absorbance values to a best fit relationship.

3.3 Water Determinations

The quantitative determination of water in the 32 samples comprising the regression, was done using three different methods to contrast reported results. These

methods are described below and the results are discussed in Chapter 4.

3.3.1 Method I The first method uses absorbance data with the assumption that the band strength for the 1.9 μ m coefficient is approximately equal to that of the 2.2 μ m coefficient. The 1.9 μ m band is a combination band with 1 mode of H₂O, an OH⁻ stretch, and an HOH bend. Similarly, the 2.2 μ m band is a combination band with an OH⁻ stretch, and an OH⁻ bend. The assumption that the coefficients are approximately equal, therefore, is based upon the similarity in band strength, band character, and vibrational mode (Clark, pers. comm., 1994). The water determinations using this method are shown in Table VI.

3.3.2 Method II The second method of water determinations involved using the molar absorptivities reported by Newman et al. (1986). The assumption made in this case is that the absorptivities for silicic glasses should be constant. The concentration of total water, derived from Bouguer - Beer's Law (Table VII), was calculated using the equation,

$$c = (18.02 * A) / \epsilon \rho d$$

(where 18.02 gm/mole is the molecular weight of H₂O).

Table VI - Water Determinations - Method I

Sample Name	File #	%H ₂ O*m=ABS.	Wt.% Molec. Water	Wt.% Hydroxyl	Wt.% Man. H ₂ O
Arroyo Hondo Obsidian	4897	0.006	0.21	0.08	0.29
Arroyo Hondo Perilite	4909	0.054	2.29	0.41	2.70
Askja Volcanic Glass	4921	0.003	0.00	0.15	0.15
Bearhead Pitchstone	4933	0.077	3.00	0.86	3.86
Big Pine Obsidian	4969	0.004	0.06	0.12	0.18
Big Pine Perilite	4981	0.058	2.44	0.46	2.90
Big Glass Mountain Pumice	4957	0.005	0.00	0.26	0.26
Big Glass Mountain Obsidian	4945	0.002	0.00	0.10	0.10
Canovas Obsidian	5005	0.004	0.07	0.14	0.21
Canovas Perilite	5029	0.058	2.52	0.38	2.90
Japan Dacite	5065	0.002	0.00	0.11	0.11
Macusanite Glass	5101	0.005	0.03	0.20	0.23
Medicine Lk. Hoffman Obsidian	5125	0.007	0.14	0.19	0.33
No Agua Obsidian 35125	5161	0.006	0.07	0.24	0.31
No Agua Perilite 35125	5185	0.046	1.97	0.33	2.30
No Agua Grefco HW Obsidian	5425	0.010	0.15	0.35	0.50
No Agua Grefco Perilite 35093	5053	0.060	2.54	0.46	3.00
No Agua Perilite 351216	5173	0.060	2.66	0.34	3.00
Olancha2 Obsidian	5221	0.019	0.41	0.54	0.95
Olancha2 Perilite	5233	0.062	2.47	0.63	3.10
Panum Grey Glass	5245	0.006	0.00	0.31	0.31
Panum Obsidian	5257	0.005	0.04	0.21	0.25
Priest Mountain Obsidian	5269	0.003	0.00	0.17	0.17
Priest Mountain Perilite	5281	0.078	3.18	0.72	3.90
Superior Obsidian	5293	0.005	0.05	0.18	0.23
Superior Perilite	5305	0.068	2.73	0.67	3.40
Thomas Obsidian	5317	0.005	0.00	0.24	0.24
Xalazaquilla Obsidian	5377	0.002	0.02	0.10	0.12
Xalazaquilla Obsidian	5389	0.002	0.02	0.10	0.12
Xalazaquilla Perilite	5401	0.062	2.61	0.49	3.10
Xalazaquilla HW Obsidian	5353	0.020	0.19	0.79	0.98
Libyan Desert Glass	5077	0.001	0.00	0.07	0.07

Table VII - Method II - Absorption Coefficients taken from Newman et al. (1986)

Sample Name	File #	2.2µm Coeff. 1.9µm ⁻¹ m	2.2µm ⁻¹ 0m	moles OH	1.9µm Coeff. imoles H ₂ O	% H ₂ O	%OH	Total % IR H ₂ O	Total % Man. H ₂ O
Arroyo Hondo Obsidian	4897	1.73	0.0020	0.0008	1.61	0.021	0.37	0.13	0.50
Arroyo Hondo Perilite	4909	1.73	0.0088	0.0016	1.61	0.092	1.65	0.27	1.92
Askja Volcanic Glass	4921	1.73	0.0000	0.0004	1.61	0.000	0.00	0.06	0.06
Bearhead Pitchstone	4933	1.73	0.0078	0.0022	1.61	0.081	1.46	0.37	1.84
Big Pine Obsidian	4969	1.73	0.0005	0.0012	1.61	0.005	0.10	0.19	0.29
Big Pine Perilite	4981	1.73	0.0081	0.0015	1.61	0.084	1.52	0.26	1.78
Big Glass Mountain Pumice	4957	1.73	0.0000	0.0005	1.61	0.000	0.00	0.08	0.08
Big Glass Mountain Obsidian	4945	1.73	0.0000	0.0003	1.61	0.000	0.00	0.05	0.05
Canovas Obsidian	5005	1.73	0.0007	0.0013	1.61	0.007	0.13	0.22	0.35
Canovas Perilite	5029	1.73	0.0094	0.0014	1.61	0.098	1.77	0.24	2.01
Japan Dacite	5065	1.73	0.0000	0.0003	1.61	0.000	0.00	0.05	0.05
Macusanite Glass	5101	1.73	0.0002	0.0012	1.61	0.002	0.04	0.19	0.23
Medicine Lk. Hoffman Obsidian	5125	1.73	0.0005	0.0006	1.61	0.005	0.09	0.10	0.19
No Agua Obsidian 35125	5161	1.73	0.0006	0.0019	1.61	0.006	0.10	0.32	0.43
No Agua Perilite 35125	5185	1.73	0.0075	0.0013	1.61	0.078	1.41	0.21	1.62
No Agua Grefco HW Obsidian	5425	1.73	0.0008	0.0020	1.61	0.009	0.15	0.33	0.48
No Agua Grefco Perilite 35093	5053	1.73	0.0082	0.0015	1.61	0.085	1.53	0.25	1.78
No Agua Perilite 351216	5173	1.73	0.0075	0.0010	1.61	0.078	1.40	0.16	1.56
Olancha2 Obsidian	5221	1.73	0.0019	0.0025	1.61	0.019	0.35	0.41	0.76
Olancha2 Perilite	5233	1.73	0.0113	0.0029	1.61	0.117	2.11	0.48	2.59
Panum Grey Glass	5245	1.73	0.0000	0.0011	1.61	0.000	0.00	0.18	0.18
Panum Obsidian	5257	1.73	0.0004	0.0019	1.61	0.004	0.07	0.31	0.38
Priest Mountain Obsidian	5269	1.73	0.0000	0.0006	1.61	0.000	0.00	0.11	0.11
Priest Mountain Perilite	5281	1.73	0.0074	0.0017	1.61	0.077	1.38	0.28	1.66
Superior Obsidian	5293	1.73	0.0002	0.0009	1.61	0.002	0.04	0.16	0.20
Superior Perilite	5305	1.73	0.0133	0.0032	1.61	0.139	2.49	0.54	3.04
Thomas Obsidian	5317	1.73	0.0000	0.0002	1.61	0.000	0.00	0.04	0.04
Xalazaquilla Obsidian	5377	1.73	0.0003	0.0018	1.61	0.003	0.06	0.30	0.36
Xalazaquilla Obsidian	5389	1.73	0.0004	0.0018	1.61	0.004	0.07	0.30	0.38
Xalazaquilla Perilite	5401	1.73	0.0078	0.0014	1.61	0.081	1.45	0.24	1.69
Xalazaquilla HW Obsidian	5353	1.73	0.0011	0.0045	1.61	0.011	0.21	0.76	0.96
Libyan Desert Glass	5077	1.73	0.0000	0.0003	1.61	0.000	0.00	0.06	0.06

3.3.3 Method III The third method of water determinations were made by calculating the absorption coefficient for each sample individually (Table VIII). The following equation was used to calculate the absorption coefficient,

$$\varepsilon = (18.02 \cdot A) / \rho d c.$$

The absorption coefficients were used to calculate the weight percent of OH (beginning with the samples where the absorbance of molecular water species = 0). The concentration of total water was determined by the following relationships:

$$A_{1.9+2.2\mu\text{m}} = A_{1.9\mu\text{m}} + A_{2.2\mu\text{m}}$$

and

$$A = \varepsilon k c.$$

From these equations it follows that:

$$c_{\text{Total H}_2\text{O}} \varepsilon_{1.9+2.2\mu\text{m Man.}} = c_{\text{H}_2\text{O}} \varepsilon_{1.9\mu\text{m}} + c_{\text{OH}} \varepsilon_{2.2\mu\text{m}}$$

$$c_{\text{H}_2\text{O}} \varepsilon_{1.9\mu\text{m IR}} = c_{\text{Total H}_2\text{O}} \varepsilon_{1.9+2.2\mu\text{m}} - c_{\text{OH}} \varepsilon_{2.2\mu\text{m}}$$

and

$$c_{\text{OH}} \varepsilon_{2.2\mu\text{m IR}} = c_{\text{Total H}_2\text{O}} \varepsilon_{1.9+2.2\mu\text{m}} - c_{\text{H}_2\text{O}} \varepsilon_{1.9\mu\text{m}}$$

where $c_{\text{H}_2\text{O}}$ and c_{OH} are the fractions of water species distributed throughout the rock.

The absorption coefficient and the fraction of each water species can, thus, be derived from this relationship using the known manometric water concentrations. The total infrared water concentrations of $c_{\text{Total H}_2\text{O}}$ ($\text{H}_2\text{O} + \text{OH}^-$) can also be determined for samples which have $c_{\text{H}_2\text{O}1.9\mu\text{m}} = 0$.

Table VIII - Method III - Absorption Coefficients - IR/Manometric H₂O

Obsidian-Perlite Pairs	File #	Coeff. 1.9+2.2 um	Coeff. 2.2 um	Coeff. 1.9 um	moles H ₂ O	moles OH	Wt. % H ₂ O	Wt. % OH	Total % IR H ₂ O	Total % Man H ₂ O
Arroyo Hondo Obsidian	4897	7.46	1.98	5.48	0.002	0.014	0.04	0.25	0.29	0.29
Arroyo Hondo Perlite	4909	7.06	4.44	2.62	0.137	0.014	2.47	0.23	2.77	2.70
Big Pine Obsidian	4969	7.19	4.87	2.32	0.002	0.009	0.03	0.15	0.19	0.18
Big Pine Perlite	4981	6.23	3.98	2.25	0.147	0.015	2.65	0.25	2.91	2.90
Canovas Obsidian	5005	7.42	4.75	2.68	0.002	0.011	0.03	0.18	0.22	0.21
Canovas Perlite	5029	6.34	3.72	2.61	0.147	0.015	2.65	0.25	3.23	2.90
No Agua Obsidian 35125	5161	6.13	4.68	1.45	0.003	0.015	0.05	0.26	0.32	0.31
No Agua Perlite 35125	5185	6.74	4.11	2.63	0.117	0.012	2.10	0.20	2.45	2.30
Olancha2 Obsidian	5221	3.53	1.96	1.57	0.008	0.048	0.14	0.81	0.98	0.95
Olancha2 Perlite	5233	9.88	6.96	2.92	0.158	0.016	2.84	0.26	2.69	3.10
Priest Mountain Obsidian	5269	2.84	2.84	0.00	0.000	0.009	0.00	0.14	0.14	0.17
Priest Mountain Perlite	5281	4.71	3.19	1.52	0.198	0.020	3.57	0.33	3.61	3.90
Superior Obsidian	5293	3.92	3.09	0.84	0.002	0.012	0.03	0.20	0.24	0.23
Superior Perlite	5305	10.29	7.14	3.15	0.173	0.017	3.11	0.29	3.02	3.40
Xalazaquilla Obsidian	5389	14.00	11.45	2.54	0.001	0.006	0.02	0.10	0.13	0.12
Xalazaquilla Obsidian	5377	13.46	11.45	2.01	0.001	0.006	0.02	0.10	0.13	0.12
Xalazaquilla Perlite	5401	5.49	3.48	2.01	0.158	0.016	2.84	0.26	3.15	3.10
Unpaired Samples										
Askja Obsidian	4921	1.81	1.81	0.00	0.000	0.008	0.00	0.13	0.13	0.15
Bearhead Pitchstone	4933	5.98	4.35	1.63	0.196	0.019	3.53	0.33	3.16	3.86
Big Glass Mountain Obsidian	4945	2.42	2.42	0.00	0.000	0.005	0.00	0.09	0.09	0.10
Big Glass Mountain Pumice	4957	1.39	1.39	0.00	0.000	0.013	0.00	0.22	0.22	0.26
Japan Dacite	5065	2.06	2.06	0.00	0.000	0.006	0.00	0.09	0.09	0.11
Macusanite Glass	5101	4.51	3.81	0.70	0.002	0.012	0.03	0.20	0.24	0.23
Medicine Lk. Hoffman Obsidian	5125	2.54	1.42	1.12	0.003	0.017	0.05	0.28	0.34	0.33
No Agua Grefco Perlite 35093	5053	5.88	3.70	2.18	0.153	0.015	2.75	0.26	3.08	3.00
No Agua Perlite 351216	5173	4.41	2.40	2.01	0.153	0.015	2.75	0.26	3.61	3.00
Panum Grey Glass	5245	2.58	2.58	0.00	0.000	0.015	0.00	0.26	0.26	0.31
Panum Obsidian	5257	6.84	5.62	1.22	0.002	0.013	0.04	0.21	0.26	0.25
Thomas Obsidian	5317	0.76	0.76	0.00	0.000	0.012	0.00	0.20	0.20	0.24
Unpaired HW Obsidian										
No Agua Grefco HW Obsidian	5425	4.28	2.96	1.32	0.004	0.025	0.07	0.43	0.52	0.50
Xalazaquilla HW Obsidian	5353	4.40	3.50	0.90	0.008	0.049	0.15	0.83	1.02	0.98
Other Glass										
Libyan Desert Glass	5077	3.67	3.67	0.00	0.000	0.004	0.00	0.06	0.06	0.07

A plot of total infrared water against total manometric water gives a 1:1 slope, indicating good agreement between manometric and infrared spectroscopic techniques for determining the water contents of obsidians ($< 0.99\%$ H₂O) (Figure 10). All samples, obsidians and perlites are plotted in Figure 11.

3.3.4 Unknowns Infrared spectra of the 15 samples with unknown total water concentrations were measured as described above. The total water concentrations (Table IX) were calculated using Method III, but because manometric water concentrations were not available, total water concentrations were derived from the linear relationship between absorbance and calibrated manometric water.

3.3.5 Geochemical Data A total of 26 samples, with data from the sources enumerated in "Methods" above, are reported in mole percent (Table X). These data were used to calculate the molecular combinations and ratios discussed in Chapters 4 and 5. The degree of alumina saturation is shown in Table XI.

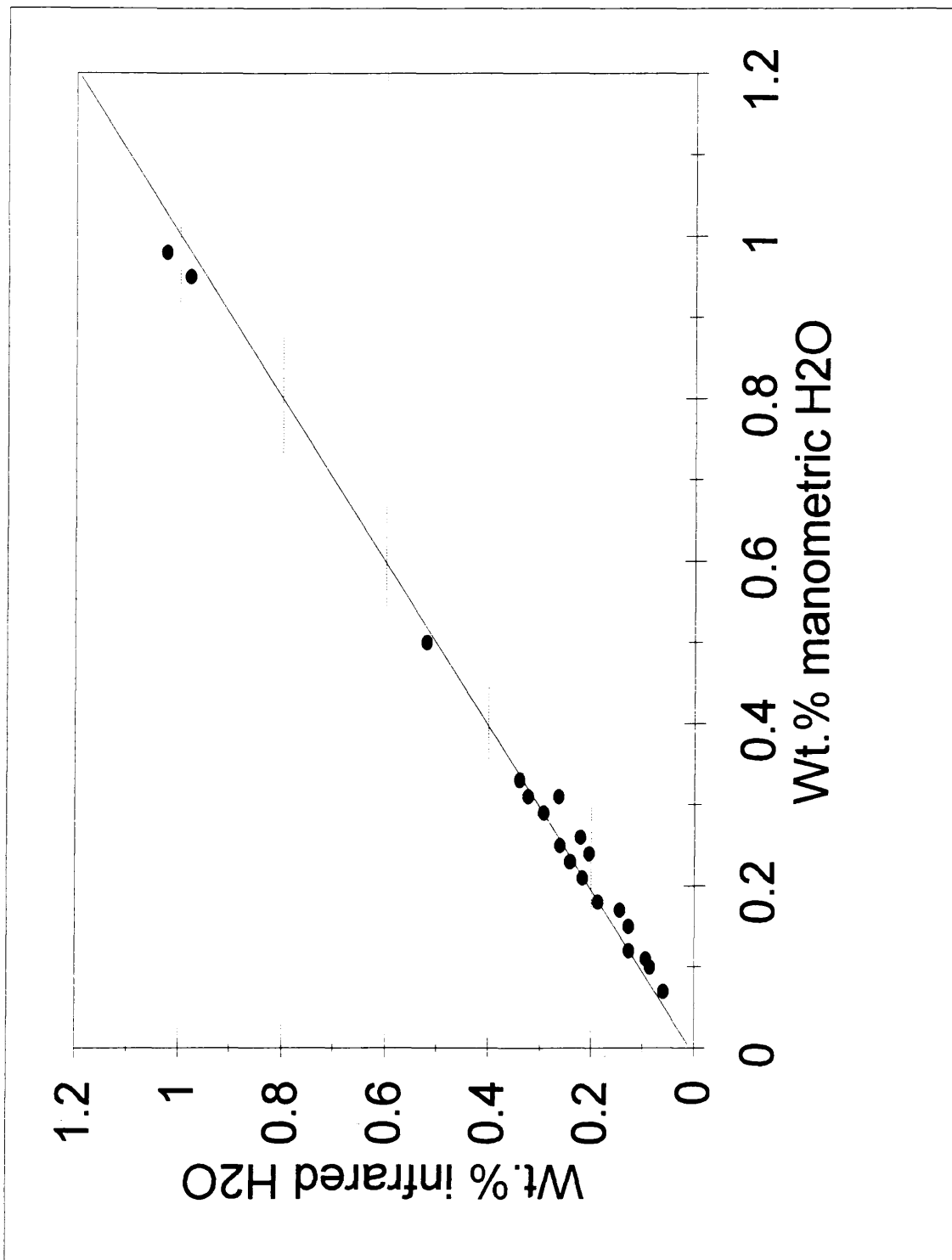


Figure 10. IR H₂O (wt.%) versus Manometric H₂O (obsidian)

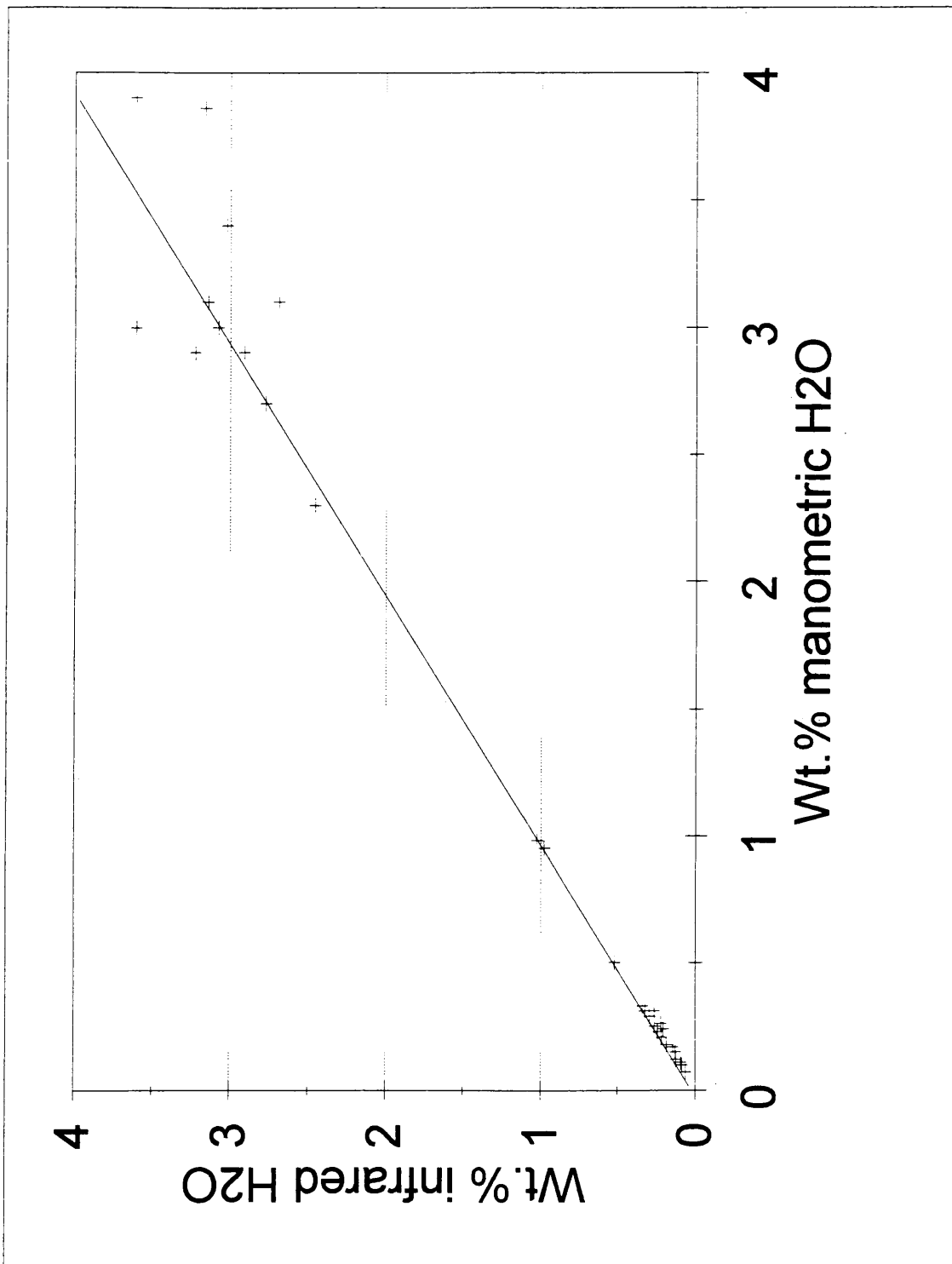


Figure 11. IR H₂O (wt. %) versus Manometric H₂O (obsidian & perlite)

Table IX - Water Determinations - Unknowns

Sample Name	File#	Coef. 2.2 um	Coef. 1.9 um	moles OH	moles H2O	Wt.% molec. H2O	Wt.% OH	Wt.% Total H2O
Bald Mountain Obsidian/Perlite	5437	4.41	2.71	0.01	0.10	1.74	0.16	1.91
Bald Mountain Perlite	5449	4.26	2.72	0.02	0.16	2.80	0.26	3.06
Black Springs Obsidian	5461	0.00	1.22	0.00	0.02	0.32	0.06	0.38
Black Springs 87-10 44-54' Perlite	5473	2.57	2.90	0.01	0.08	1.39	0.13	1.52
Coso Obsidian	5485	0.01	1.19	0.06	0.01	0.15	1.03	1.18
Cudahy Perlite	5497	4.22	2.73	0.01	0.13	2.32	0.22	2.53
Cudahy Mahogany Obsidian	5509	0.00	0.00	0.00	0.00	0.02	0.01	0.03
Delamar Perlite	5521	5.48	2.59	0.01	0.10	1.83	0.17	2.00
Frazier Canyon Perlite/Pitchstone	5533	6.13	2.52	0.02	0.16	2.85	0.26	3.11
Mount Floyd Smith Tank Obsidian	5545	0.00	0.00	0.00	0.00	0.08	0.03	0.12
Mount Floyd York Perlite	5557	4.64	2.68	0.01	0.11	1.95	0.18	2.13
Opal Beaver County Utah	5569	7.10	2.42	0.01	0.13	2.27	0.21	2.48
Peralta Perlite	5581	5.10	2.63	0.01	0.12	2.24	0.21	2.45
Peralta Obsidian	5593	0.00	1.97	0.02	0.01	0.11	0.34	0.44
Ruby Mountain Pitchstone/Perlite	5605	5.11	2.63	0.01	0.13	2.36	0.22	2.58

Table X - Chemistry - H₂O & OH⁻ (mole%)

Sample Name/Type	mole% H ₂ O	mole% OH	mole% SiO ₂	mole% Al ₂ O ₃	mole% Fe ₂ O ₃	mole% FeO	mole% MgO	mole% CaO	mole% Na ₂ O	mole% K ₂ O	Total mole%
Obsidian - Perifite Pairs											
Big Pine Obsidian	0.11	0.57	82.04	8.39	0.15	0.30	0.08	0.61	4.72	3.02	100.00
Big Pine Perifite	8.85	0.88	74.57	7.68	0.28	0.00	0.13	0.64	3.88	3.10	100.00
No Agua Obsidian 35125	0.18	1.00	82.12	9.36	0.35	0.00	0.16	0.64	3.27	2.91	100.00
No Agua Perifite 35125	7.21	0.73	75.71	8.07	0.17	0.19	0.08	0.93	4.05	2.87	100.00
Superior Obsidian	0.11	0.76	82.53	8.05	0.14	0.32	0.14	0.55	4.23	3.17	100.00
Superior Perifite	10.13	1.00	73.28	7.46	0.22	0.00	0.47	0.85	3.75	2.84	100.00
Unpaired Samples											
Askia Glass	0.00	0.50	78.14	8.16	0.45	2.57	1.18	3.12	4.29	1.59	100.00
Bald Mountain Obsidian/Perifite	5.90	0.57	77.72	7.65	0.13	0.28	0.08	0.49	4.24	2.94	100.00
Big Glass Mtn. Obsidian	0.00	0.35	80.06	9.01	0.17	1.18	0.42	1.44	4.36	3.02	100.00
Black Springs Obsidian	1.14	0.23	81.59	8.25	0.12	0.52	0.05	0.89	3.97	3.24	100.00
Canovas Obsidian	0.11	0.69	82.44	8.10	0.16	0.27	0.10	0.50	4.51	3.13	100.00
Cudahy Mahogany Obsidian	0.07	0.04	82.63	8.32	0.14	0.51	0.03	0.92	4.07	3.27	100.00
Macusanite	0.11	0.78	77.63	10.44	0.55	0.38	0.29	2.44	3.51	3.88	100.00
Medicine Lk. Hoffman Obsidian	0.18	1.07	79.33	8.92	0.17	1.17	0.42	1.43	4.32	2.99	100.00
Mt. Floyd Smith Tank Obsidian	0.29	0.11	83.00	8.15	0.35	0.00	0.10	0.51	4.40	3.08	100.00
Mt. Floyd York Perifite	6.76	0.66	77.09	7.59	0.36	0.00	0.12	0.48	3.83	3.10	100.00
Panum Grey Glass	0.00	0.99	82.34	7.94	0.13	0.68	0.03	0.60	4.13	3.15	100.00
Panum Obsidian	0.14	0.80	82.38	7.94	0.13	0.68	0.03	0.60	4.13	3.15	100.00
Priest Mtn. Obsidian	0.00	0.53	82.36	7.76	0.18	1.03	0.16	1.24	4.46	2.27	100.00
Xalazaquilla Obsidian	0.07	0.38	82.88	7.83	0.17	0.73	0.02	0.49	4.05	3.38	100.00
Xalazaquilla Obsidian	0.07	0.38	82.88	7.83	0.17	0.73	0.02	0.49	4.05	3.38	100.00
High Water Glasses											
No Agua Grefco HW Obsidian	0.26	1.67	81.72	8.60	0.29	0.00	0.49	1.53	2.45	3.01	100.00
Olancha2 Obsidian	0.49	3.02	80.00	7.90	0.14	0.40	0.08	0.52	4.61	2.85	100.00
Xalazaquilla HW Obsidian	0.53	3.13	79.05	8.81	0.04	0.46	0.05	0.55	4.57	2.82	100.00

Table XI - Alumina Saturation

Sample Name	mole% H ₂ O	mole% OH	(CaO+Na ₂ O+K ₂ O)/Al ₂ O ₃	Alumina Saturation
Askja Glass	0.00	0.50	1.10	Subaluminous
Bald Mountain Obsidian/Perlite	5.90	0.57	1.00	Subaluminous
Big Pine Obsidian	0.11	0.57	1.00	Subaluminous
Big Glass Mtn. Obsidian	0.00	0.35	0.98	Subaluminous
Big Pine Perlite	8.85	0.88	0.99	Subaluminous
Black Springs Obsidian	1.14	0.23	0.98	Subaluminous
Canovas Obsidian	0.11	0.69	1.00	Subaluminous
Cudahy Mahogany Obsidian	0.07	0.04	0.99	Subaluminous
Macusanite	0.11	0.78	0.94	Metaluminous
Medicine Lk. Hoffman Obsidian	0.18	1.07	0.98	Subaluminous
Mt. Floyd Smith Tank Obsidian	0.29	0.11	0.98	Subaluminous
Mt. Floyd York Perlite	6.76	0.66	0.98	Subaluminous
No Agua Perlite 35125	7.21	0.73	0.97	Subaluminous
No Agua Grefco HW Obsidian	0.26	1.67	0.81	Peraluminous
No Agua Obs. 35125	0.18	1.00	0.73	Peraluminous
Olancha2 Obsidian	0.49	3.02	1.01	Subaluminous
Panum Grey Glass	0.00	0.99	0.99	Subaluminous
Panum Obsidian	0.14	0.80	0.99	Subaluminous
Priest Mtn. Obsidian	0.00	0.53	1.03	Subaluminous
Superior Obsidian	0.11	0.76	0.99	Subaluminous
Superior Perlite	10.13	1.00	1.00	Subaluminous
Xalazaquilla HW Obsidian	0.53	3.13	0.90	Peraluminous
Xalazaquilla Obsidian	0.07	0.38	1.01	Subaluminous
Xalazaquilla Obsidian	0.07	0.38	1.01	Subaluminous

Chapter 4. RESULTS

4.1 Data Treatment

Method III (Table IX) shows results that are in agreement with the hypothesis that hydroxyl saturation reaches an upper limit at approximately 0.30 weight % (Friedman, 1993). This is the approximate maximum total H_2O ($H_2O + OH^-$) in unaltered obsidian, beyond which molecular water becomes dominant. In contrast, the hydroxyl concentrations calculated using Method I exceed this limit (Table VI).

Method II gave large discrepancies at high and low total IR water ($H_2O + OH^-$) concentrations (Table VII). Water concentrations were lower than the manometric values over the ranges 0.04-0.23 and 1.66-3.04 % IR H_2O , while samples in the range 0.23-0.96 % IR H_2O showed good agreement. The latter samples are influenced by molecular water, which increases above the upper limit of hydration for hydroxyl contents in obsidians. The large discrepancy within the perlite range suggests that at high molecular water concentrations (2 - 5%) the absorption coefficients decrease, and for these samples the 1.9 μ m band is significantly stronger than the 2.2 μ m band. In this light, the use of Method III is justified as the preferred technique to derive quantitative data because the relative concentration of molecular water is accommodated by individual calculations which are adjusted according to the actual amount of absorption occurring.

The quantitative results derived from Method III show some variation with respect

to hydroxyl water contents. This variation is shown by the 3 samples, Olancha2, Xalazaquilla, and Grefco, which have anomalously high hydroxyl concentrations. These "high water obsidians" have hydroxyl water contents of 0.95, 0.98, and 0.50 wt.% OH⁻, respectively. In contrast, the maximum hydroxyl content predicted experimentally is 0.19 wt.% OH⁻ (Sykes et al., 1993). The "high water" outliers must be explained by variations in temperature or pressure which are not related to the simple cooling of a magma with an abnormally high volatile fraction.

4.2 Data Analysis

In order to characterize the process of hydration, the emphasis of this analysis is placed upon the corresponding changes in chemistry accompanying hydration. The method adopted for this analysis was to plot chemical parameters against the water contents and species. As discussed earlier, combined errors are on the order of $\pm 0.05\%$ for water, and typically better than 1 - 2 wt.% (relative) for major elements. All data presented, reported as mole%, are taken from Table X. The data examined belong to the groups listed below:

1.) Water Species

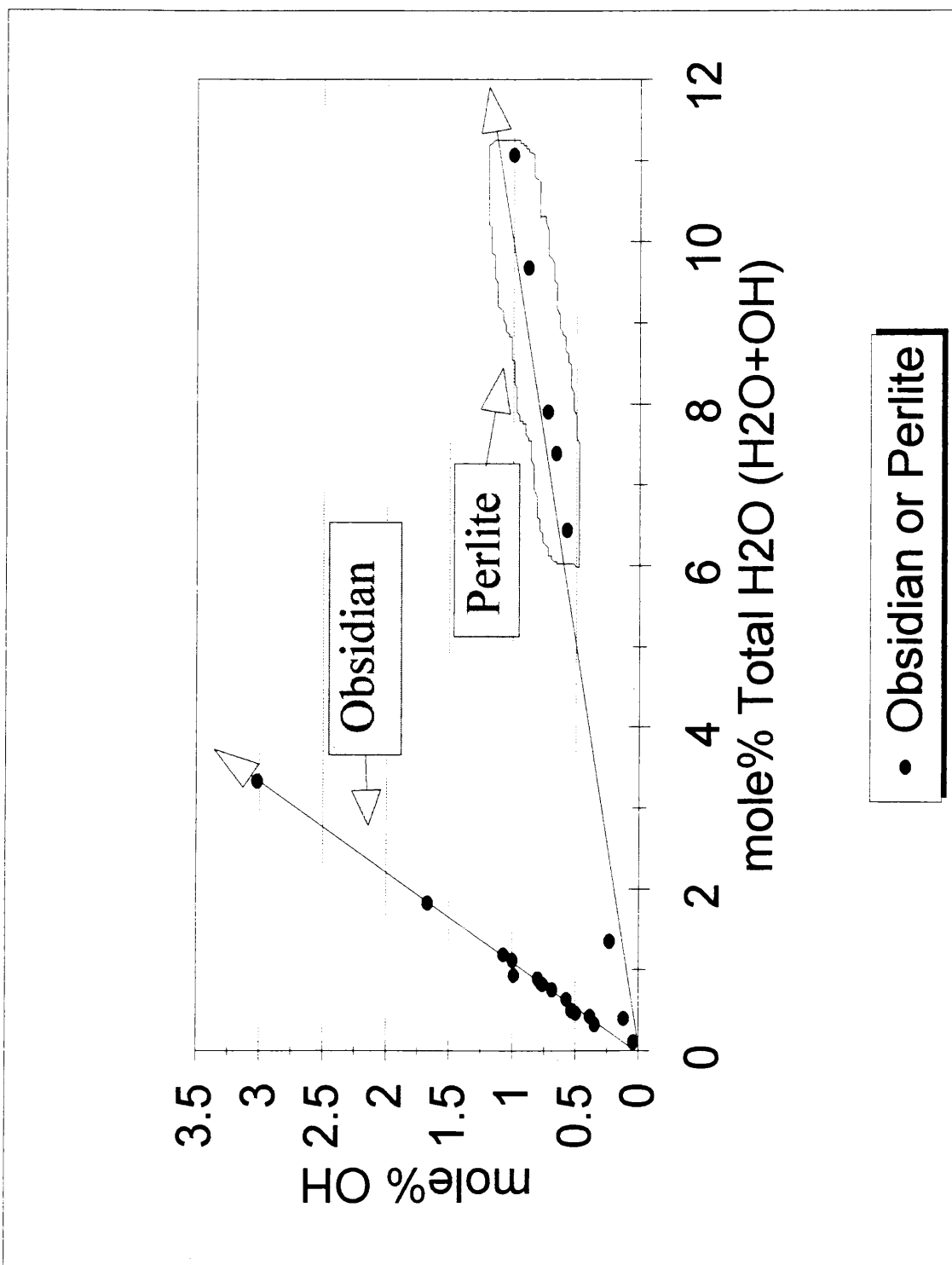
- a.) Hydroxyl water species (mole% OH⁻)
- b.) Molecular water species (mole% H₂O)
- c.) Total water species (mole% Total H₂O, molecular + hydroxyl species)

- 2.) Network Formers (SiO_2 and Al_2O_3)
- 3.) Network Modifiers (Na_2O , K_2O , CaO , and MgO)
- 4.) Network Modifiers : Network Former - $\text{CaO} + \text{NaO} + \text{K}_2\text{O} / \text{Al}_2\text{O}_3$

4.2.1 Water Species A plot of mole% OH against mole% total H_2O ($\text{H}_2\text{O} + \text{OH}^-$) shows 2 trends (Figure 12). Hydroxyl contents in obsidian are generally less than ~ 1 mole%, except in the 3 samples of high water obsidian, and the total water content is generally below 1.75%. Molecular water in perlites increases linearly to a maximum hydroxyl content of ~ 1 mole%, at a molecular water content of 10 mole%.

4.2.2 Network Formers A plot of SiO_2 (mole%) versus OH^- (Figure 13) shows 2 major trends. With decreasing SiO_2 , OH^- in both hydrated obsidian and perlite increases slightly, while OH^- contents increase rapidly in hydrated obsidian. A plot of SiO_2 (mole%) versus H_2O shows a pronounced decrease in SiO_2 content with an increase in molecular water in perlite (Figure 14).

The plot of Al_2O_3 (mole%) versus OH^- (Figure 15) shows 2 trends, although these are not well defined with respect to specific hydration types. The best defined trend shows a decrease in Al_2O_3 with increasing in OH^- in a group of samples which includes obsidian and perlite. The second, weaker, trend consists of hydrated obsidians, and



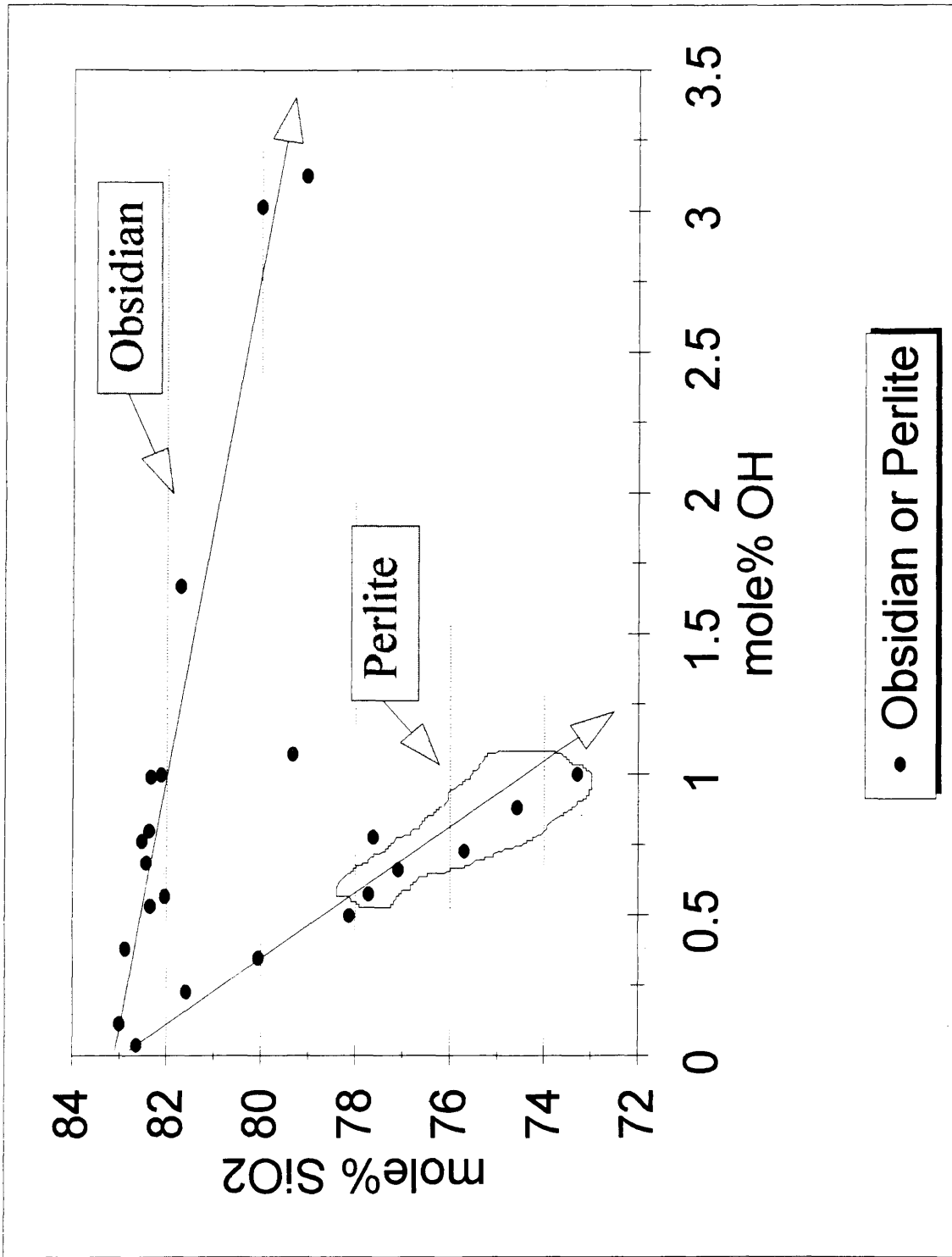


Figure 13. SiO₂ (mole%) versus OH⁻

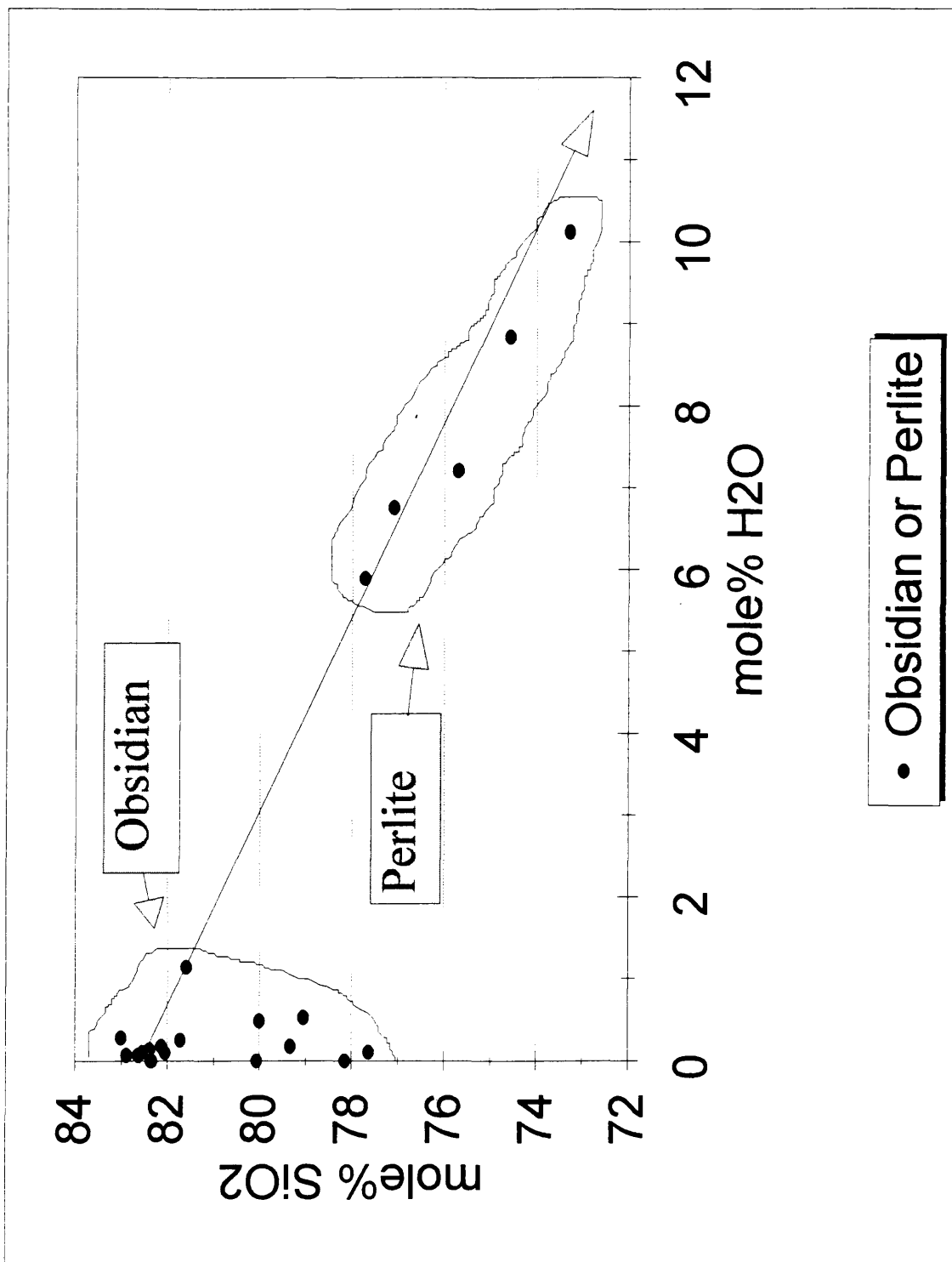


Figure 14. SiO₂ (mole%) versus H₂O

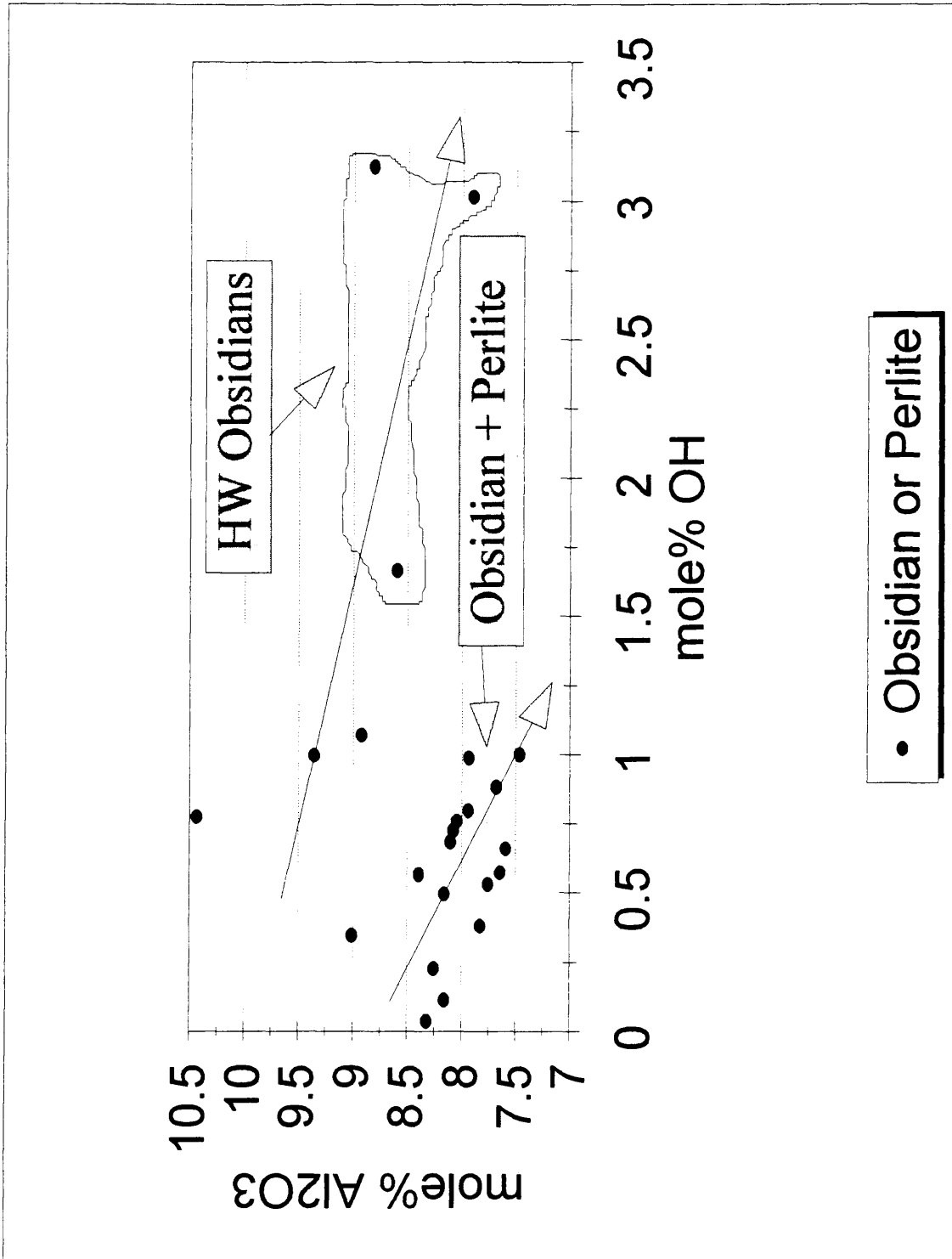


Figure 15. Al₂O₃ (mole%) versus OH

includes the 3 samples of high water obsidian. A plot of Al_2O_3 (mole%) versus H_2O shows a gradual decrease in Al_2O_3 associated with higher H_2O in perlite (Figure 16).

$\text{SiO}_2 + \text{Al}_2\text{O}_3$ (mole%) versus OH (Figure 17) shows two general trends as seen in the plot of SiO_2 versus OH^- (Figure 13). This plot shows that at low concentrations, network formers decrease rapidly with respect to a modest increase in OH^- contents in perlite. The highest network former value within the perlite group is the obsidian sample from Askja (91% $\text{SiO}_2 + \text{Al}_2\text{O}_3$, and 0.05% OH^-). The obsidian group is characterized by higher $\text{SiO}_2 + \text{Al}_2\text{O}_3$ concentrations, which gradually decrease with respect to an increase over wide range in OH^- . This range is extended to higher OH^- values by the three high water obsidians.

4.2.3 Network Modifiers K belongs to the group of low field strength elements.

This group is comprised of elements with a high ratio of ionic radius to ionic charge. K has the largest ionic radius of the elements in this group. A plot of K_2O (mole%) versus OH^- shows a decrease in K_2O content with respect to an increase in OH^- for both obsidian and perlite (Figure 18). A plot of K_2O (mole%) against H_2O shows that K_2O decreases as H_2O increases in the perlite group (Figure 19). At higher K_2O concentrations, this trend includes the two obsidian samples, Cudahy Mahogany Obsidian (3.27% K_2O , 0.07% H_2O) and Black Springs Obsidian (3.24% K_2O , and 1.14% H_2O).

Na also belongs to the group of low field strength elements, but has a smaller

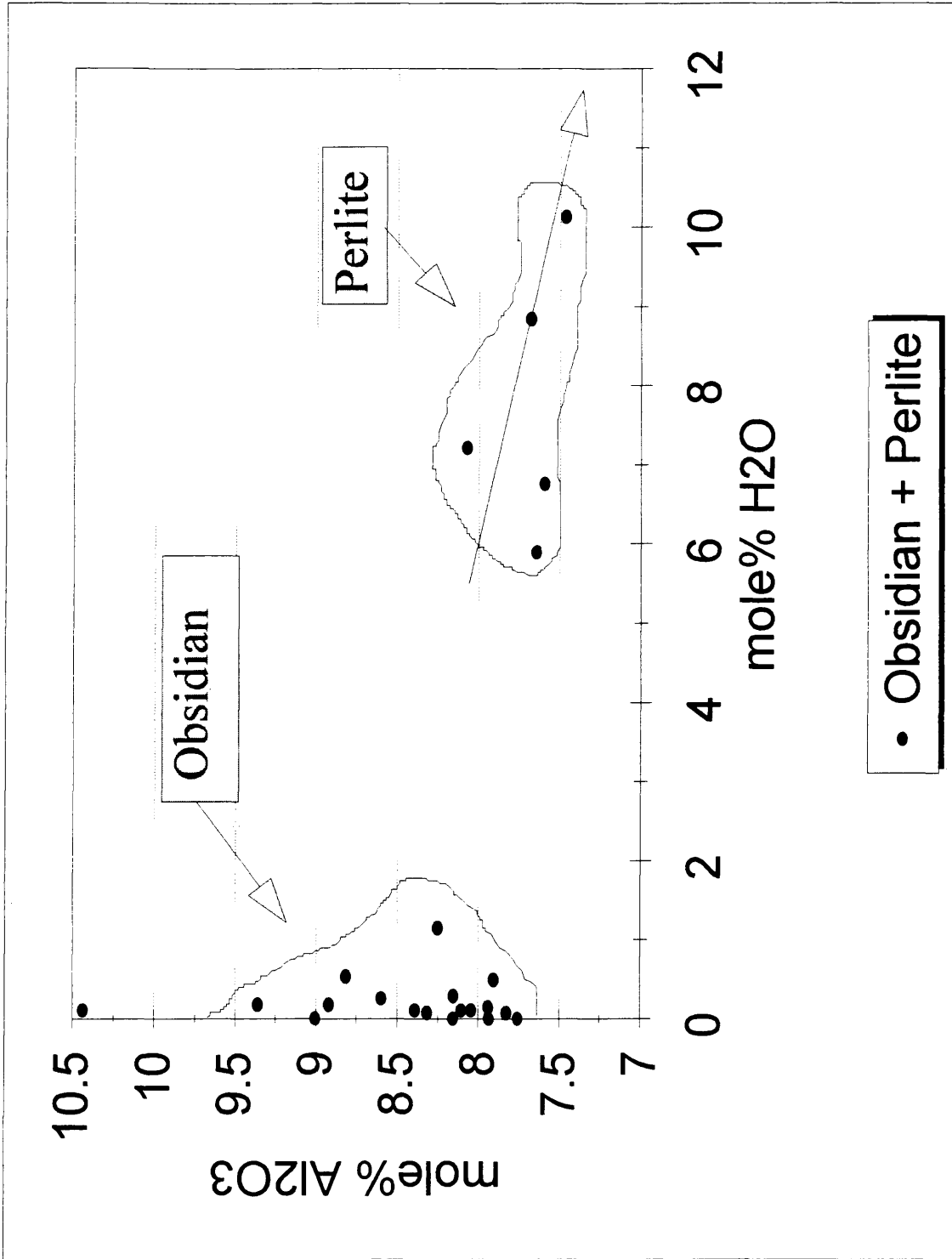


Figure 16. Al₂O₃ (mole%) versus H₂O

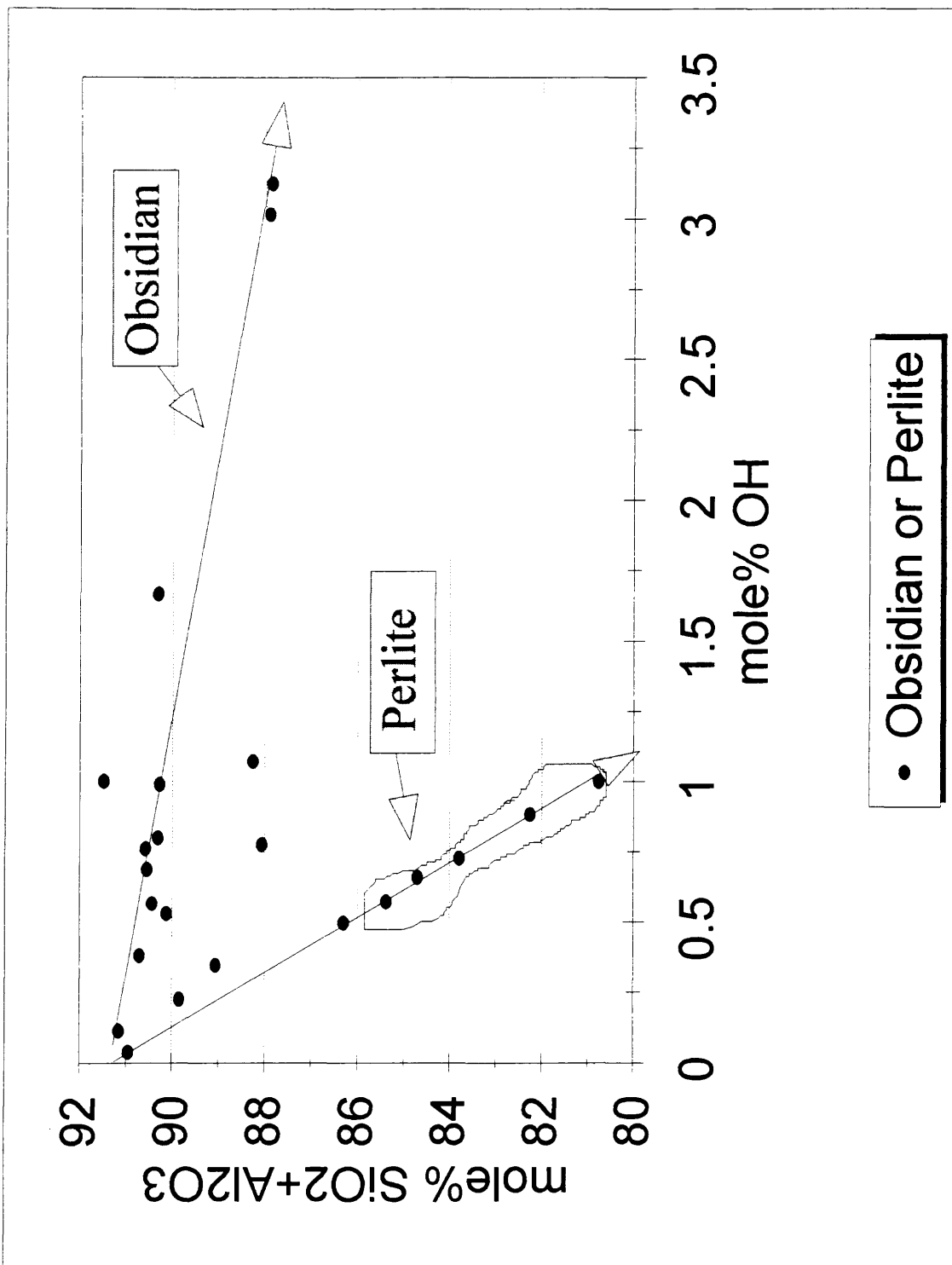


Figure 17. SiO₂ + Al₂O₃ (mole%) versus OH

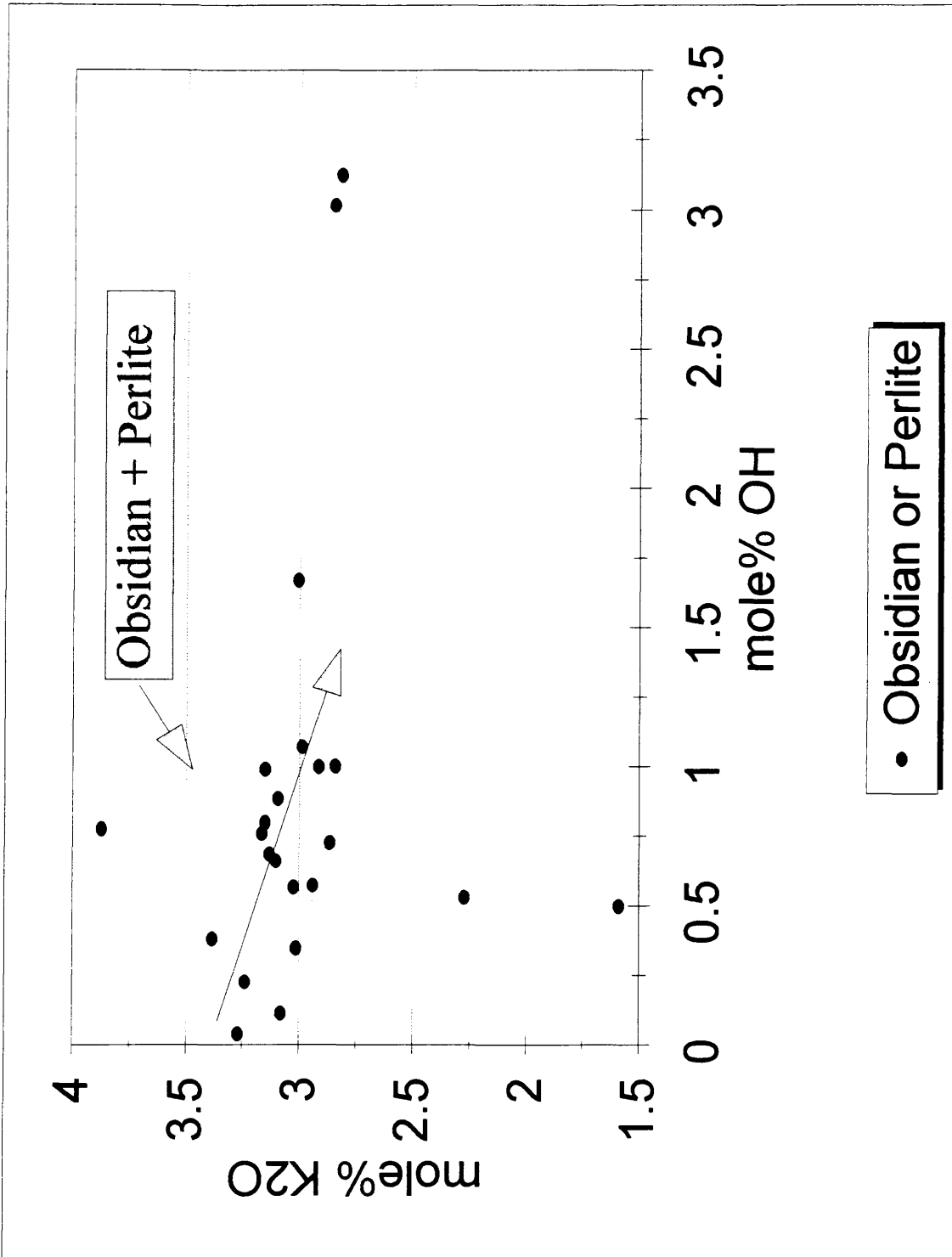


Figure 18. K₂O (mole%) versus OH

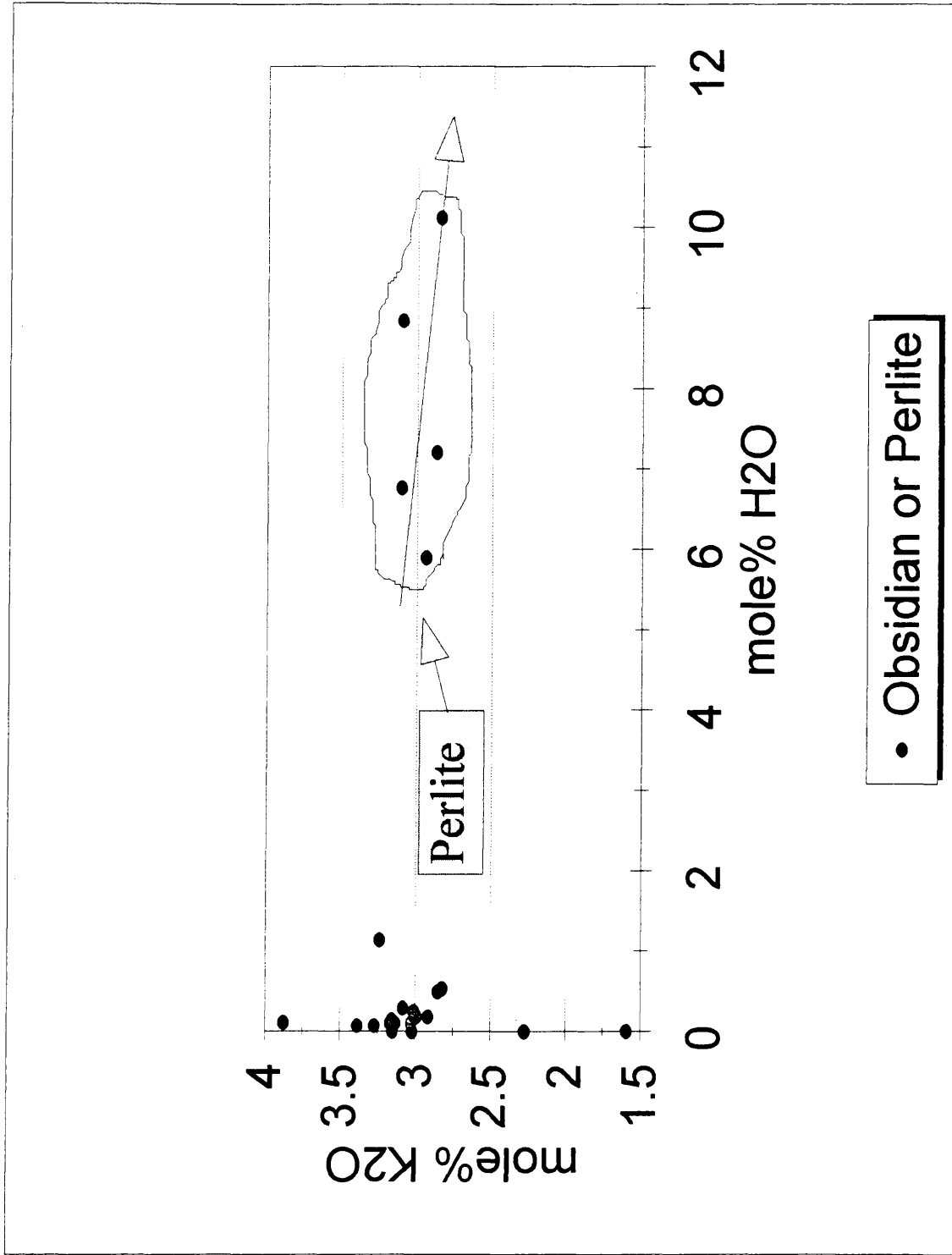


Figure 19. K₂O (mole%) versus H₂O

ionic radius than K. A plot of Na₂O (mole%) versus OH⁻ shows that Na₂O decreases as OH⁻ increases (Figure 20). The two high water obsidian samples, Olancha2 and Xalazaquilla, show elevated Na₂O and OH⁻ contents and are not included with the trend. The high water Grefco obsidian sample plots along the low Na₂O end of the trend. A plot of Na₂O (mole%) against H₂O shows a decrease in Na₂O content as H₂O increases (Figure 21). Two of the high water obsidian samples, Olancha2 and Xalapazquilla, and a sample of Canovas obsidian are included in this trend and plot close to zero mole% H₂O.

Ca has a smaller ionic radii than the elements in the group described above. A plot of CaO (mole%) against OH⁻ does not show any distinct trends (Figure 22). In contrast, a plot of CaO (mole%) against H₂O shows that CaO gradually increases as the H₂O content increases in the perlite group (Figure 23).

The Mg⁺² ion has a smaller ionic radius than Ca⁺². A plot of MgO (mole%) against OH⁻ does not show any trends in any of the three groups of glasses (Figure 24). Similarly, a plot of MgO (mole%) against H₂O does not show any trends (Figure 25).

4.2.4 Network Modifiers : Network Former The aluminum saturation principle was used to classify the glasses in this data set (Table XI). The groups are listed below:

Peraluminous - $[Al_2O_3] > [Na_2O+K_2O+CaO]$

Metaluminous - $[Al_2O_3] > [Na_2O+K_2O]$, but "usually" $< [Na_2O+K_2O+CaO]$

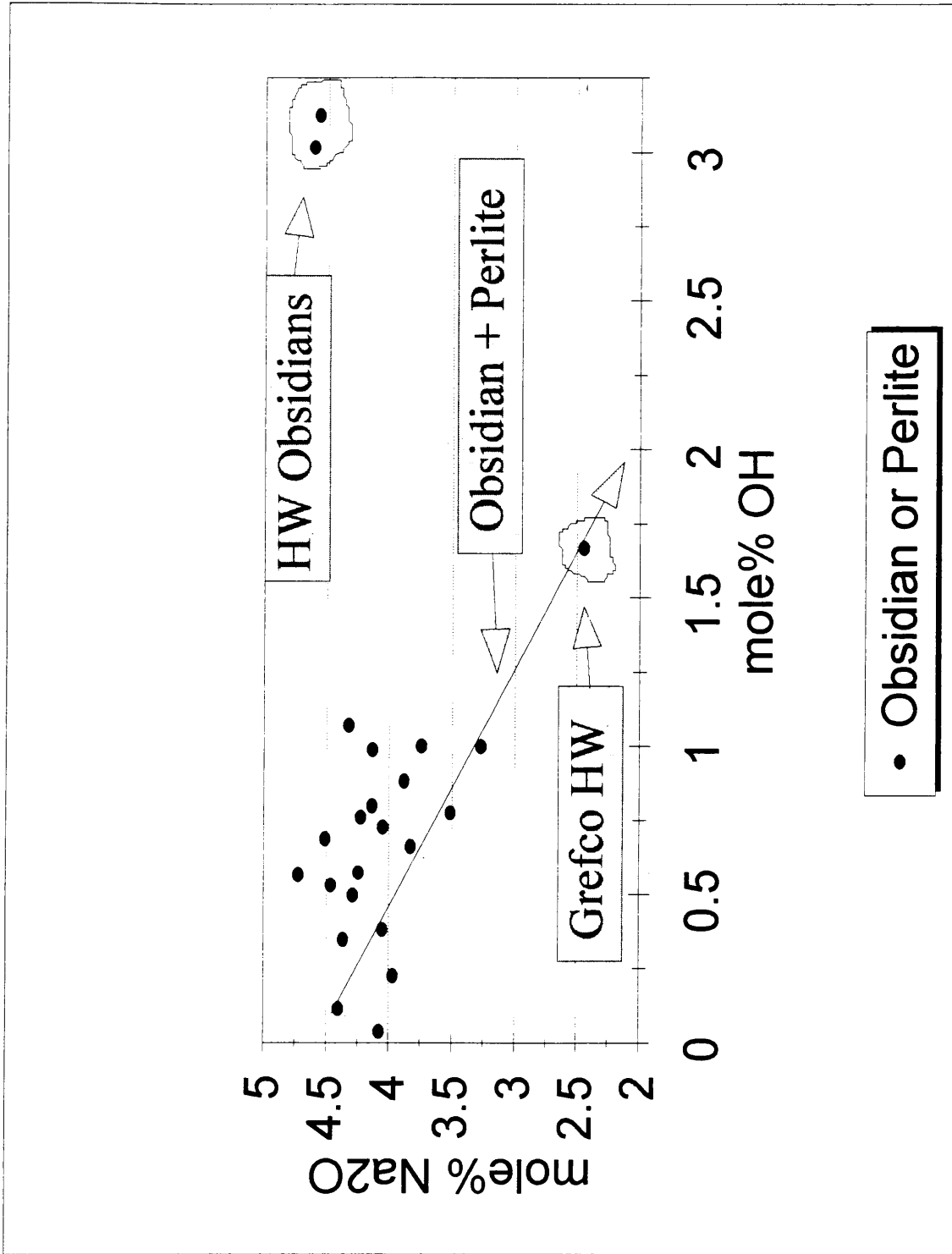


Figure 20. Na₂O (mole%) versus OH

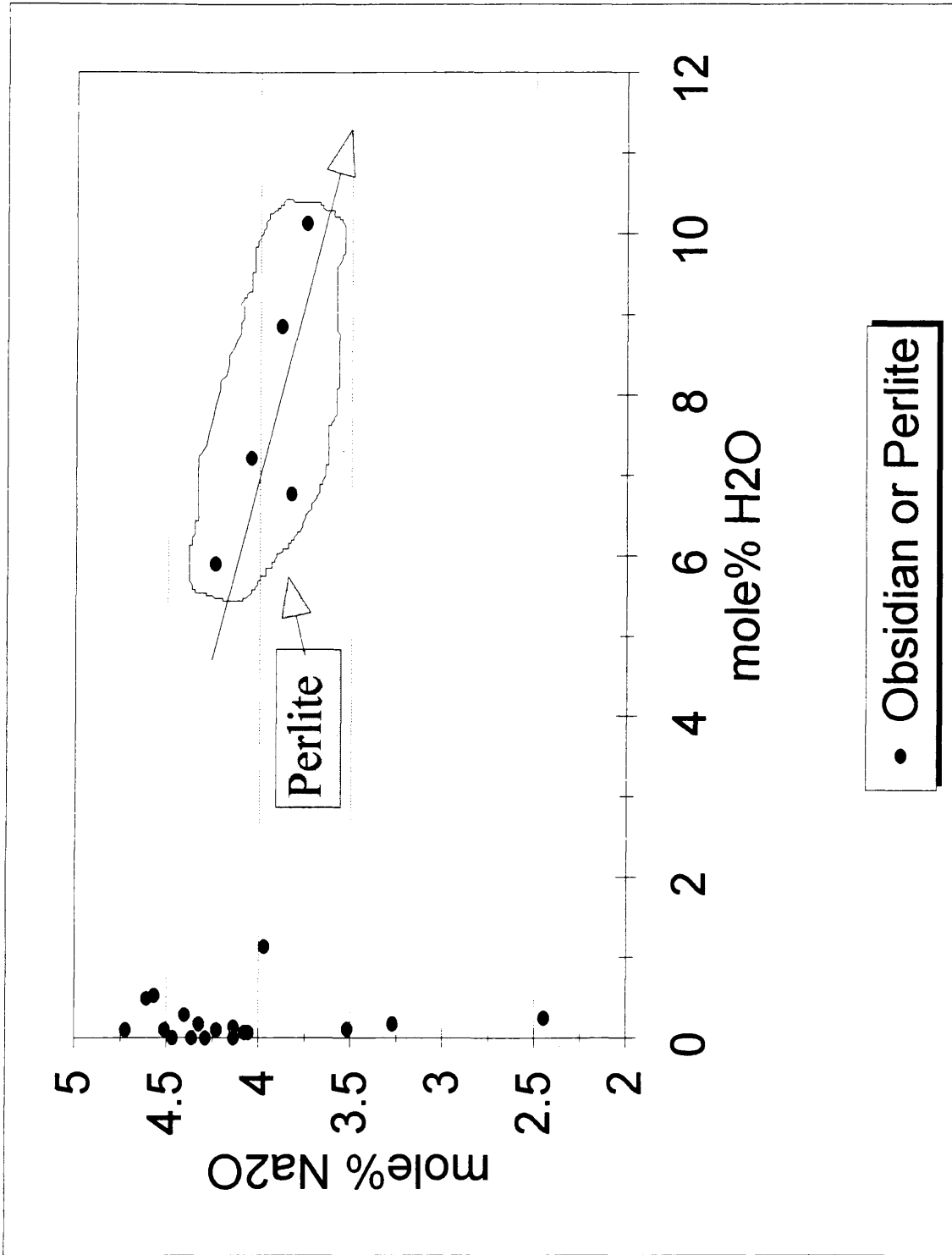


Figure 21. Na₂O (mole%) versus H₂O

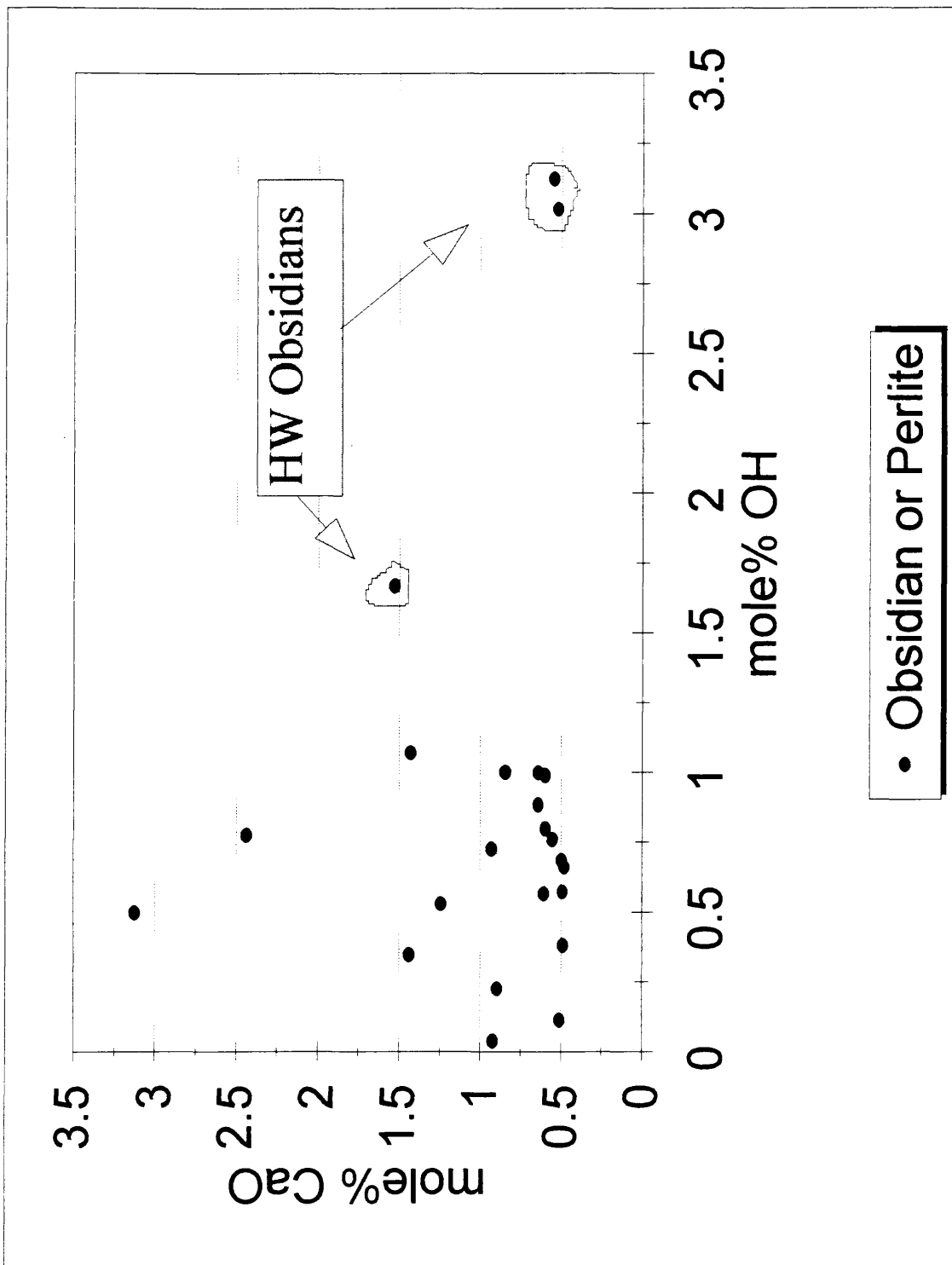


Figure 22. CaO (mole%) versus OH⁻

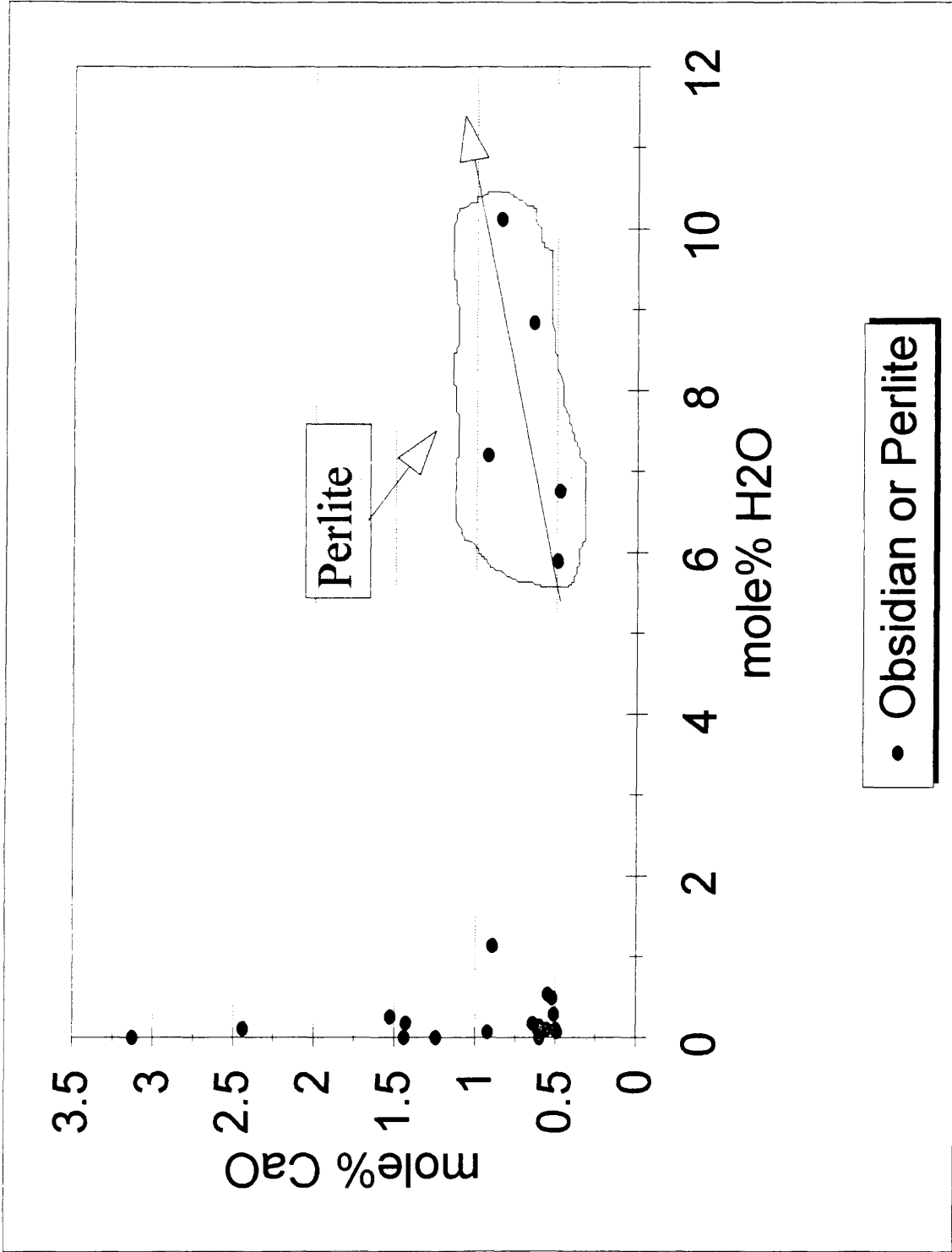


Figure 23. CaO (mole%) versus H₂O

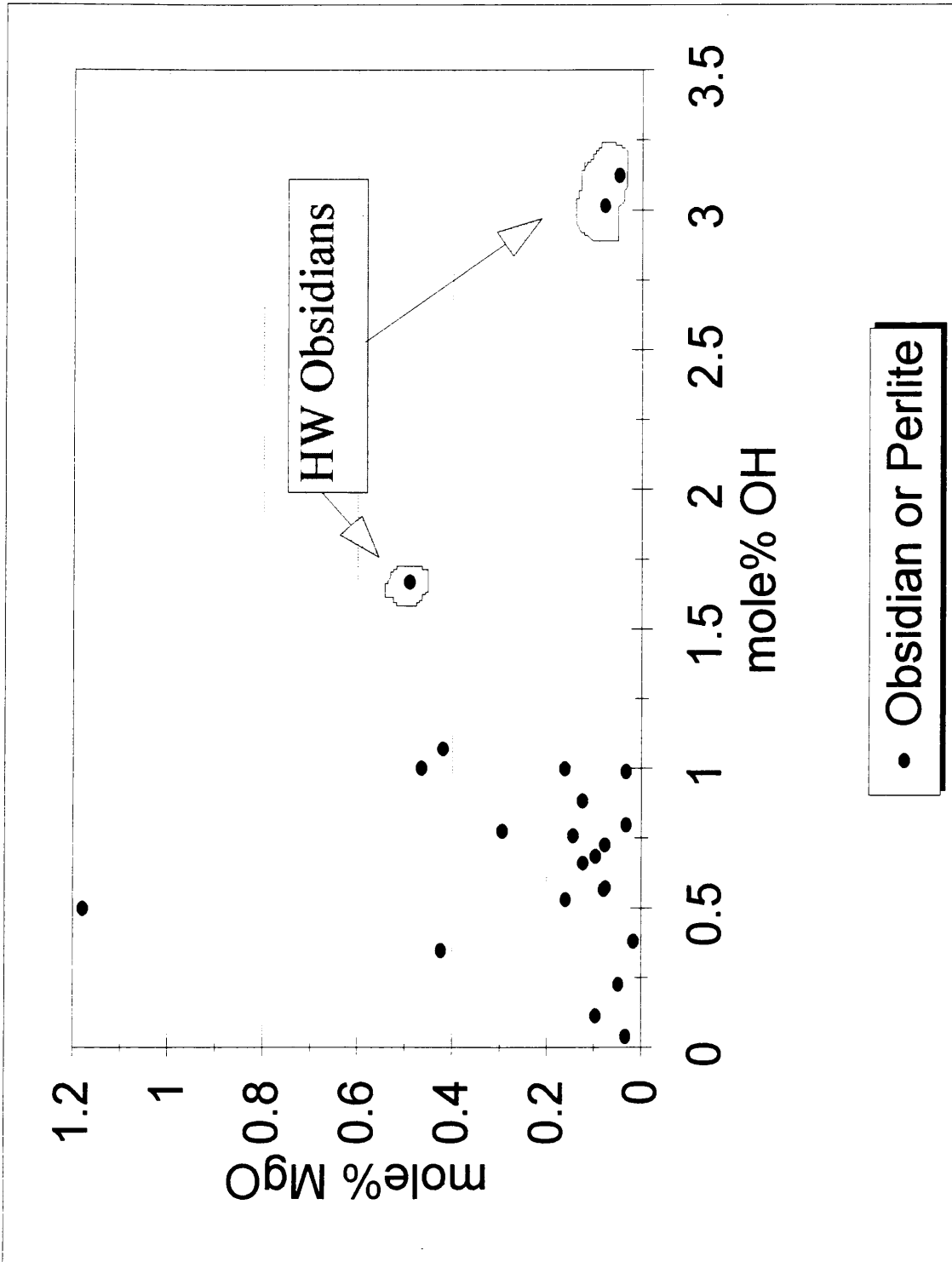


Figure 24. MgO (mole%) versus OH⁻

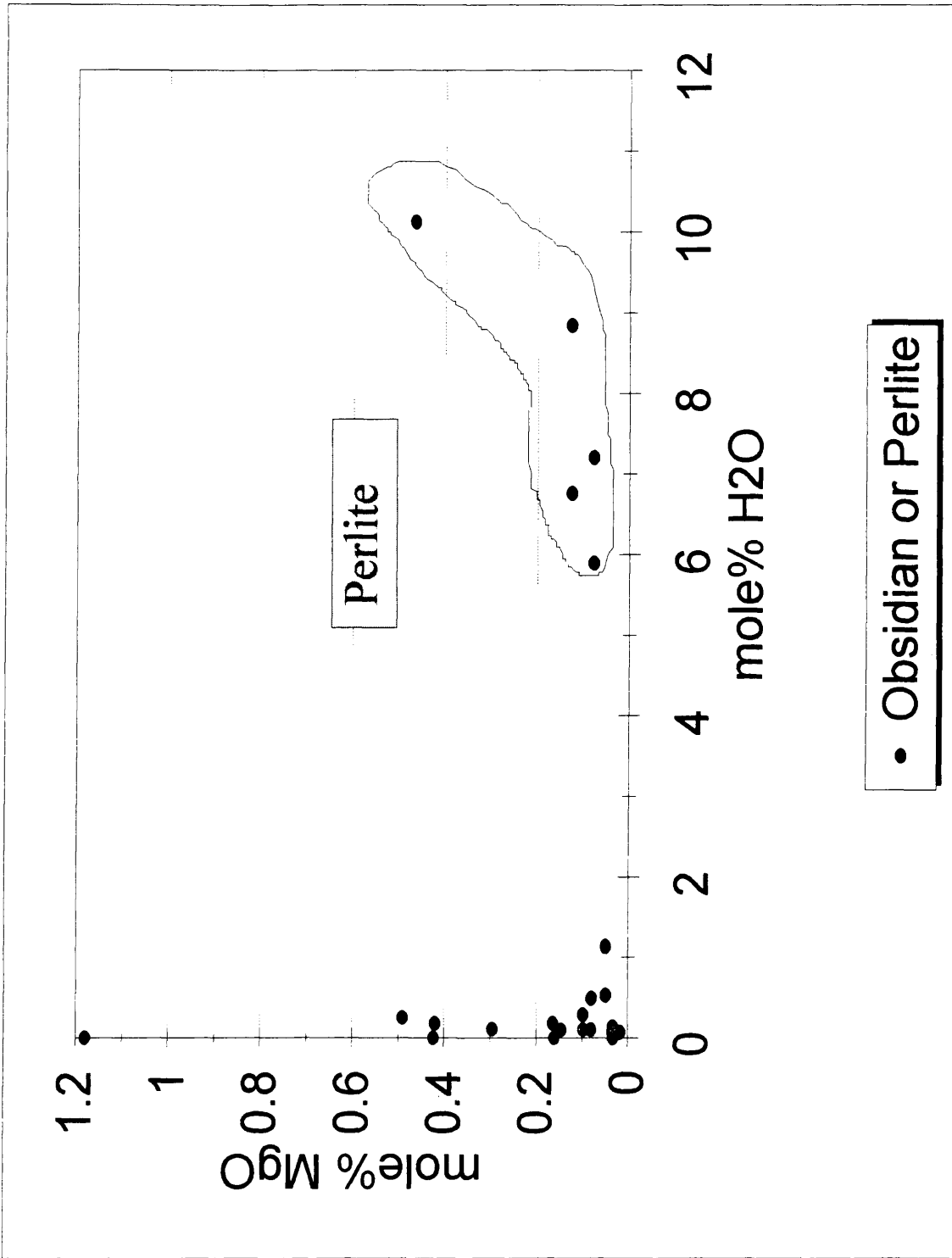


Figure 25. MgO (mole%) versus H₂O

Subaluminous - $[Al_2O_3] \simeq [Na_2O+K_2O+CaO]$

Peralkaline - $[Al_2O_3] < [Na_2O+K_2O]$

A plot of $CaO+Na_2O+K_2O/Al_2O_3$ (mole%) against OH^- shows that the samples are divided into peraluminous glasses which consist of the HW obsidians (No Agua Grefco, Olancha2, and Xalazaquilla), and subaluminous glasses which consist of the remaining obsidian and perlite samples (Figure 26). A plot of $CaO+Na_2O+K_2O/Al_2O_3$ (mole%) against H_2O shows that the perlite - obsidian pairs may be plotted as two distinct groups (Figure 27). $CaO+Na_2O+K_2O/Al_2O_3$ shows no change with respect to an increase in molecular water in the subaluminous group comprised of perlites. Low molecular water contents characterize the peraluminous obsidians, which consist of No Agua obsidian 35125, the HW No Agua Grefco obsidian , and the HW Xalazaquilla obsidian.

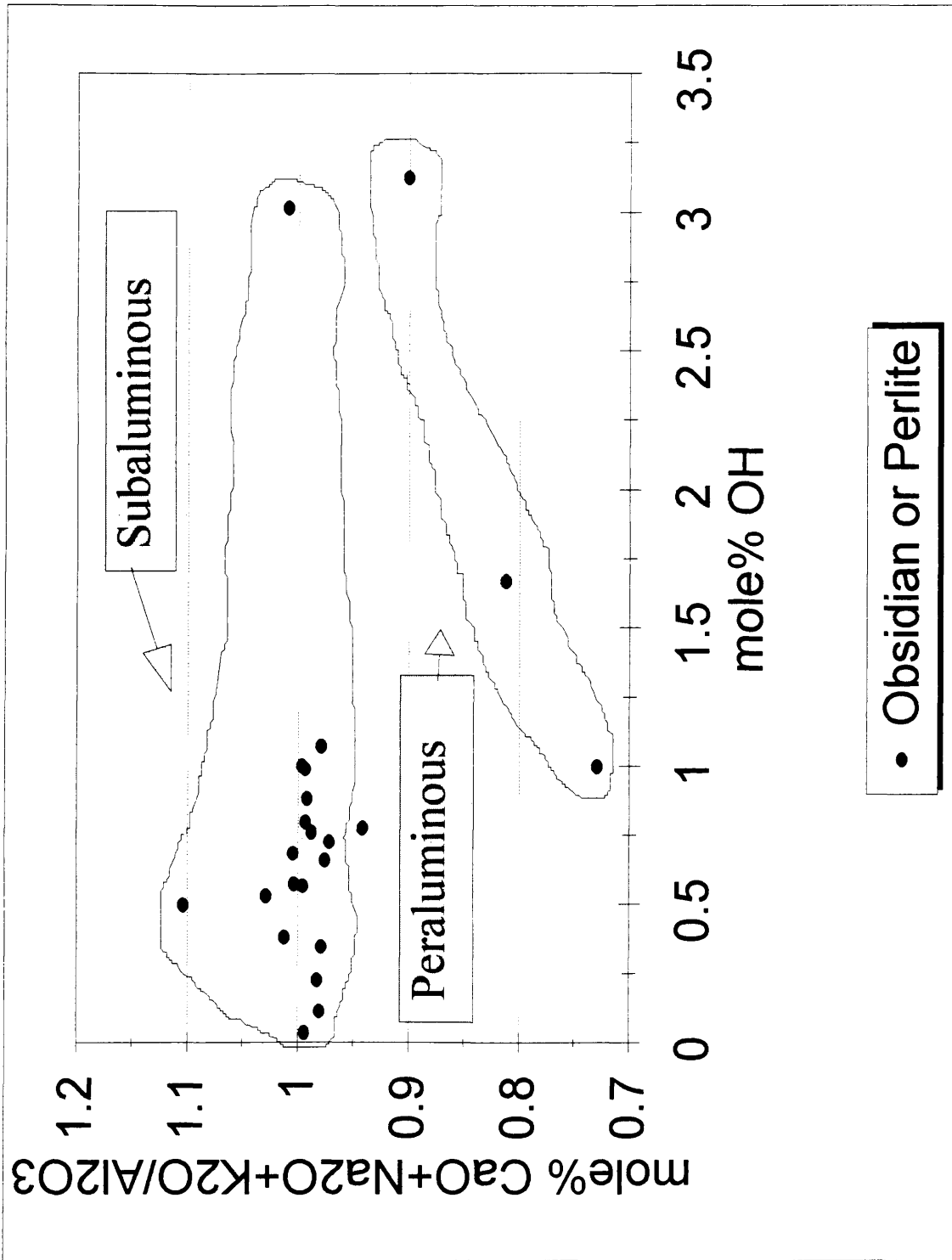


Figure 26. CaO+Na₂O+K₂O/Al₂O₃ (mole%) OH

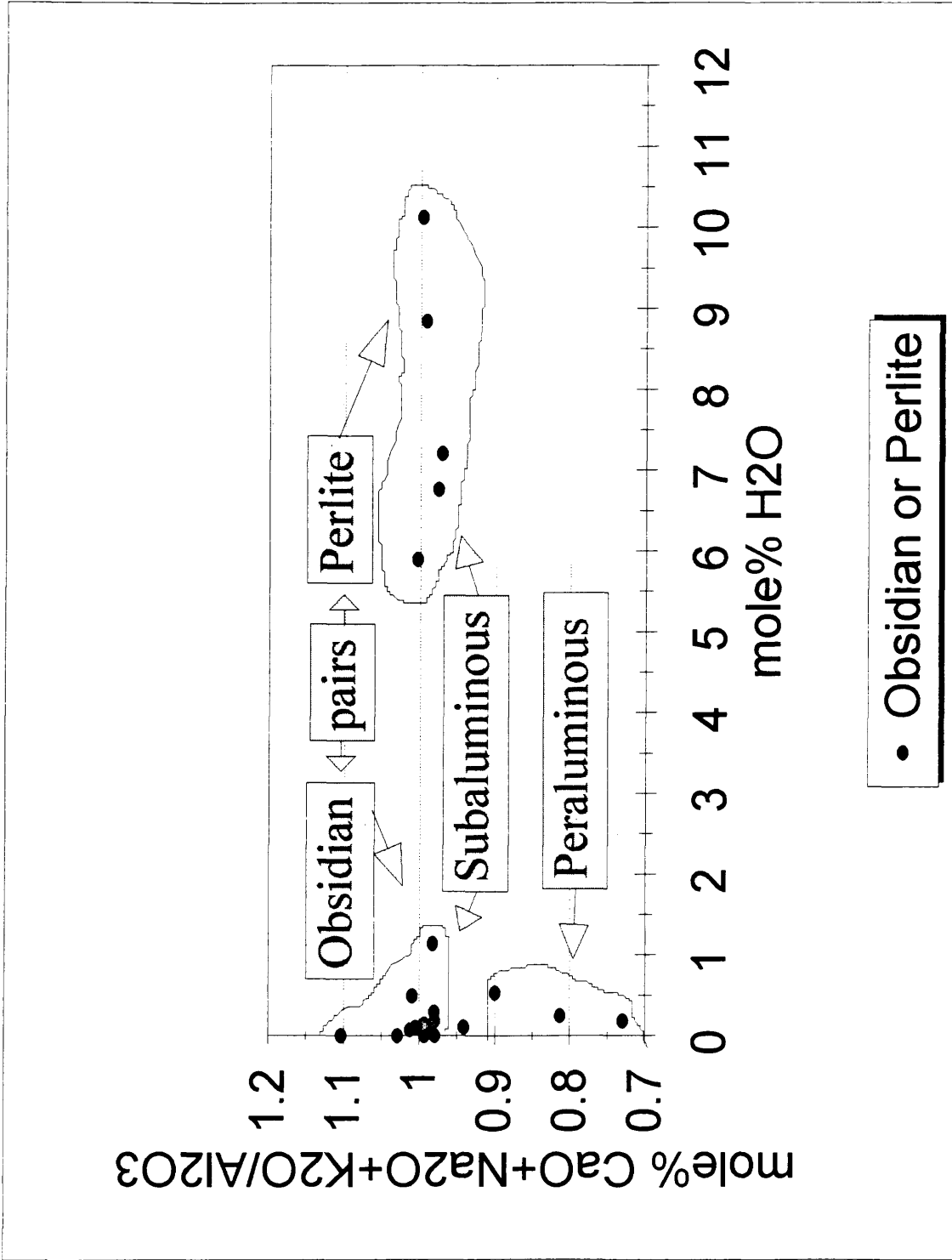


Figure 27. CaO+Na₂O+K₂O/Al₂O₃ (mole%) H₂O

Chapter 5 INTERPRETATION OF RESULTS

5.1 Hydroxyl Contents

The hydroxyl water concentrations in obsidian increase to a maximum concentration (Figure 12). This upper limit of hydroxyl concentration is predicted by mixing models (Burnham, 1975), and is characterized by a higher molecular to hydroxyl ratio than that exhibited by synthetic albite melts. The upper limit for hydroxyl water in the natural glasses observed in this study is ~ 1 mole%. This value is lower than the 30 mole% predicted experimentally for synthetic albitic glass (Sykes and Kubicki, 1993).

The "high water obsidians", Olancha2, Xalazaquilla, and Grefco, have anomalously high hydroxyl concentrations. These samples have total water contents of 0.95, 0.98, 0.50 wt.% and hydroxyl concentrations of 0.81, 0.83, and 0.43 wt.%, respectively. The "high water" obsidians may be explained by variations in temperature or pressure which are not related to the simple cooling of a magma with an abnormally high volatile fraction (Friedman, 1993). These obsidians may have been hydrated during a second stage of hydroxyl diffusion which superseded primary hydration. Intrusions of a magma into water-saturated sediments at elevated temperatures and pressures, or local hot springs activity may elevate the hydroxyl water concentration. The temperature dependence of the speciation of water was first suggested in studies of hydrated obsidian from Mono Craters (Newman et al., 1988). An experimental study by Stolper (1989)

showed that water speciation depends upon temperature and the amount of water present, and that it is reversible. A good example of water speciation is the high water obsidian-perlite pair from Olancha. This sample was taken from the contact between a volcanic dome and sedimentary rocks in the Coso Volcanic Field. This obsidian has hydroxyl water determined to be 0.81 wt.%. In contrast to the obsidian core, the perlite has 0.26 wt.% OH⁻ out of 3.10 wt.% total H₂O. These compositions suggest that secondary hydration may destroy the OH⁻ bridging, and enlarge channels for the passage of large molecules of H₂O (Ericson et al., 1976).

The sample from Coso Volcanic Field may be an example of the effect of hot springs activity upon hydration. This glass is metaluminous (Bacon et al., 1981) and is characterized by low water contents (< 0.31 wt.% total H₂O). The Coso obsidian sample submitted by Christopher Stevenson from an area near Sugarloaf Mountain, has a total water content of 1.18 wt.%. The hydroxyl water for this sample was determined to be 1.03 wt.% using IR spectroscopy. Hot spring activity is reported in this area (Friedman, pers. comm., 1994), and the alteration associated with this activity may be responsible for the abnormally high water content.

5.2 Network Formers

The role of the network formers in hydration is shown in Figures 13 - 17. The ratio of [SiO₂]/[OH⁻] is higher for obsidians (excluding the high water samples) than

perlites. This relationship suggests that the leaching of SiO_2 during secondary hydration involves initially the breakup of a Si-O-Si bridge by water vapor at the surface, dividing the Si-O-Si component into two silanol groups (Ericson et al., 1976; Drury, 1962). Water then fills the open space created and further attack begins with a proton (H^+) jump to another Si-O-Si bridge close by, breaking up the the bridge to free a hydroxyl, which will then react with Si to form silanol. Repetition of these reactions produces a net transfer in the ratio of 2:1, with re-bridging of silanol occurring. The silanol groups can react with additional molecular water to produce the reverse reaction. Leaching of Si can occur from bond breakage, as the frequency of reactions increases, and developement of new channelways, which will allow the passage of molecular water. The ratio of $[\text{SiO}_2]/[\text{H}_2\text{O}]$ is higher for obsidians than perlites, and also indicative of Si leaching. In perlites, this leaching is associated with the introduction of molecular water (Lipman, 1965).

The strong trend which shows a decrease in Al_2O_3 with respect to OH^- in obsidian, hydrated obsidian, and perlite (Figure 15) supports the network modifier role of Al (Burham, 1975; Ericson et al., 1976). This decrease in Al_2O_3 with increasing OH^- may also be associated with secondary leaching of Al by molecular water. As a network former Al has low mobility, but as a network modifier, its mobility is increased. The weaker subparallel trend of Al_2O_3 versus OH^- is comprised of three peraluminous glasses (No Agua obsidian 35125, No Agua Grefco HW obsidian, and Xalazaquilla HW obsidian) and two subaluminous glasses (Medicine Lake Hoffman obsidian and Olancha2 HW obsidian). The apparent difference in peralkalinity between the Xalapazquilla HW

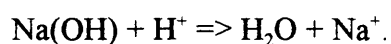
obsidian and the Olancha2 HW obsidian can be explained by the chemical changes associated with the hydration of an originally metaluminous magma (Bacon et al., 1981) of the Coso Volcanic Field.

5.3 Network Modifiers

The role of the network modifiers in hydration is shown in Figures 18 - 25. The decrease in K_2O with increasing OH^- is associated with secondary hydration in obsidian and perlite (Figure 18). The two lowest K_2O values are obsidian samples from Askja and Priest Mountain (oceanic extensional zone), and the highest value is the Macusanite glass. These outliers are easily explained by their chemistries which are characteristically low and high in alumina, respectively. The hydrated obsidians in this study do not show enrichment in K_2O , contrary to studies by Jezek and Noble (1978) and Lipman (1965). The plot of K_2O versus H_2O further supports these observations (Figure 19).

Na is another network modifier which has been employed in models describing water solubility mechanisms in synthetic albite melts (Sykes and Kubicki, 1993; Mysen, 1992; and Burham, 1975). A strong trend is shown in the plot of Na_2O versus OH^- (Figure 20). The decrease in Na_2O with an increase in OH^- establishes the role of Na^+ in the process of hydration in natural glasses. This observation is in agreement with a study by Mysen (1992) which showed that in synthetic albite melts Na-OH bonds dominate at

total H₂O contents ≤ 4 mole%. A decrease in Na₂O (mole%) is accompanied by an increase in H₂O for the perlite group. This behavior supports the conclusions of Sykes and Kubicki (1993) and Mysen (1992) in their studies of synthetic albite melts that an upper limit of total H₂O is reached, above which molecular water species become dominant over hydroxyl species. Pandya et al. (1992) present the following mechanism to explain this process:



The ratio of non-bridging oxygens to tetrahedrally coordinated cations decreases to the upper limit dominated by NaOH bonds (until all of the available cations are bonded to hydroxyls), and increases with the addition of molecular water (Mysen, 1992). The creation of channelways, which allow the passage of molecular water through the glass, can be explained by the disruption of intermediate range order through the formation of Na-OH, and the associated breakup of bridges between adjacent tetrahedra. The movement of water through the glass is accomplished by the transfer of a single H⁺ to a non-bridging O, and may also be associated with the transfer of alkalis to form complexes with the OH radical (Mysen, 1992). Figure 21 shows that Na₂O in perlite decreases as molecular water increases. Because this trend is not seen in the obsidians, it is concluded that most Na₂O is removed by secondary leaching at ambient temperatures.

The two HW obsidians, Olancha2 and Xalazaquilla, do not follow the trend shown for most obsidians with respect to hydroxyl content (Figure 20). The Grefco No Agua HW sample, however, does line up with the trend for perlites at low molecular water

contents. The significance of these relationships is not apparent, although it is possible to speculate that these glasses were hydrated by the incorporation of connate or meteoric waters into magma locally along the margins of volcanic domes in contact with water-saturated sediments. Hydration at near magmatic temperatures may somehow extend the limit of hydroxyl-dominated hydration. Perhaps the ionic exchange which takes place between the connate or meteoric waters and the magma may inhibit the migration of Na^+ out of the magma. The waters could be saline, or Na^+ could be trapped in a closed system, migrating along thermal gradients controlled by convection.

The +2 valence ions, Ca and Mg, do not show any significant trends (Figures 22-25), although there is gradual increase in what may be residual Ca in perlite with an increase in molecular water (Figure 23). The absence of any trends in this data set argues against suggestions presented by Pandya et al. (1992) in favor of the hydration of hydroxyl species involving X^{+2} cations.

5.4 Network Modifiers : Network Former

The plots of $\text{CaO}+\text{Na}_2\text{O}+\text{K}_2\text{O}/\text{Al}_2\text{O}_3$ versus OH^- and $\text{CaO}+\text{Na}_2\text{O}+\text{K}_2\text{O}/\text{Al}_2\text{O}_3$ versus H_2O show that hydration by molecular water produces a most pronounced subdivision of the subaluminous glasses into two distinct groups. These data were plotted in an attempt to contrast variations in total alkalis and Al_2O_3 to the amount of hydration of each water species. The division of the subaluminous group suggests that the combined

influence of the alkalies is balanced by the effect of Al_2O_3 . This observation argues against the proposal by Mysen (1992) that Al_2O_3 becomes dominant above the upper limit for OH^- concentration, and is dominantly associated with the hydration of molecular water.

Chapter 6. CONCLUSION

The data presented in this investigation were gathered in an attempt to use transmission IR spectroscopy to quantify the molecular water/silanol ratio in hydrated silicic volcanic glasses. These data were tabulated and analysed with respect to changes in chemistry associated with hydration. The conclusions drawn from these data are:

- 1.) Quantitative IR measurements of hydrated volcanic glasses with total or combined H₂O concentrations greater than 2 wt.% can be measured using powdered samples dispersed throughout KBr pellets. When compared to slab samples with water concentrations less than 2%, this method yields comparable results.
- 2.) Method III is a superior technique for quantitative determination of water concentration. The effect of H₂O > 2 wt.% in perlite makes it necessary to use absorption coefficients which change with the proportion of molecular to hydroxyl water. Changes in the structure of volcanic glass with increasing hydration support this approach.
- 3.) Water is bound within obsidian and perlite as hydroxyl and molecular water. At ambient temperatures and pressures, the amount of molecular water within the glass increases with increasing total or combined water (H₂O + OH⁻). Hydroxyl water species reach an upper limit of approximately 0.30 wt.% H₂O, and rarely

exceed this concentration.

4.) Hydroxyl water derived from magmatic processes can be used to estimate the magmatic character of the glass by measuring the ratio of hydroxyl to molecular water species within the glass. The data presented support the concept that primary hydration is dominated by hydroxyl water and that polymerization of the melt is controlled by the interaction of cations with hydroxyls, which may dissociate during and subsequent to quenching.

5.) There are ranges over which cations bond with hydroxyls in X-OH groups. The data suggest that the dominant bonding type is SiOH below 1 mole% OH⁻. This suggestion is based upon the division of the samples into two distinct trends for obsidians and perlite. Na⁺, K⁺, and Al³⁺ are cations which have lower electronegativities than Si⁴⁺, but compete for OH⁻ because of the greater bond strength between Si and O. The low valence state of the alkalis and hydroxyl water lend mobility to alkaline hydroxides. These compounds, therefore, can more easily migrate out of the glass during leaching and promote further breakdown of the glass through the influx of additional molecular water attacking fresh surfaces. This process describes hydration as an attack of fresh surfaces, layer by layer, along diffusion fronts, followed by the influx of molecular water along fractures developed by primary stress corrosion and enhanced by secondary processes.

REFERENCES

Acocella, J., Tomozawa, M. and Watson, E. B., 1984, The nature of dissolved water in silicate glasses and its effect on various properties, *Journal of Non-Crystalline Solids*, Vol. 65, pp. 355-372.

Aines R. D., and Rossman, G. R., 1984, Water in minerals? A peak in the infrared, *J. Geophys. Res.*, Vol. 89, No., B5, pp. 4059-407

Allen, R. L., 1988, False pyroclastic textures in altered silicic lavas, with implications for volcanic-associated mineralization, *Economic Geology*, Vol. 83, No.7, pp. 1424-1446.

Austin, G. S., and Barker, J. M., 1994, Production and Marketing of Perlite in the western United States, in Proceedings, 29th Forum on the Geology of Industrial Minerals, Long Beach California, 1993, California Bureau of Mines and Geology (in press).

Bacon, C. R., MacDonald, R., Smith, R. L., and Baedeker, P. A., 1981, Pleistocene High-Silica Rhyolites of the Coso Volcanic Field, Inyo, County, California, *J. Geophys. Res.*, Vol. 86, No. B11, pp. 10223 - 10241.

Barnes, V.E., Edwards, G., McLaughlin, W. A., Friedman, I., and Joensuu, O., 1970,

Macusanite occurrence, age and composition, *G. S. A. Bull.*, Vol. 81, pp. 1539-1546.

Bartholomew, R. F., Butler, B. L., Hoover, H. L., and Wu, C. K., 1980, Infrared spectra of a water-containing glass, *American Ceramic Society Journal*, Vol. 63, pp. 481-485.

Breese, R.O.Y., and Piper, J.R., 1985, Occurrence and origin of perlite, *Society of Mining Engineers of A.I.M. E.*, Preprint Number 85-359, 12p.

Burnham, C. W., 1975, Water and magmas; a mixing model, *Geochemica et Cosmochimica Acta*, Vol. 39, pp. 1077 - 1084.

Brinker, C.J., Brow, R.K., Tallant, D.R., and Kirkpatrick, R.J., 1990, Surface structure and chemistry of high surface area silica gels, *Special Issue of the Journal of Non-Crystalline Solids*, Vol. 120, pp. 26-33.

Carmichael, I. S. E., 1979, Glass and the Glassy Rocks, in *The Evolution of the Igneous Rocks*, Yoder, H. S. Jr., ed., Princeton University Press, Princeton, New Jersey, pp. 233-244.

Clark, R. N., 1993, *Spectrum Processing Routines*, U. S. G. S. Open File Report No. 93-595, 202p.

Crecraft, H. R., Nash, W. P., and Evans, S. H., Jr., 1981, Late Cenozoic Volcanism at Twin Peaks, Utah: Geology and Petrology, *J. Geophys. Res.*, Vol. 86, No. B11, pp. 10303-10320.

Drury T., Roberts, G.J., and Roberts, J. P., 1962, Advances in Glass Technology, Plenum Press, New York, pp. 249-254.

Ewart, A., 1971, Chemical Changes Accompanying Spherulitic Crystallization in Rhyolitic Lavas, Central Volcanic Region, New Zealand, *Mineralogical Magazine*, Vol. 38, pp. 424-434.

Fisher, R.V., and Schmincke, H.U., 1984, Pyroclastic Rocks, Springer-Verlag, Berlin, 472p.

Friedman I. and Long W., 1984, Volcanic glasses, their origins and alteration processes, *Journal of Non-crystalline Solids*, Vol. 67, Nos. 1-3, pp. 127-134.

Friedman, I., and Obradovich, J., 1981, Obsidian Hydration Dating of Volcanic Events, *Quaternary Research*, 16, pp. 37-47.

Friedman, I., and Trembour, F. W., 1978, Obsidian: The dating stone, *American Scientist*,

Vol. 66, No. 1, pp. 44-51.

Friedman, I., and Parker, C. J., 1969, Libyan desert glass: its viscosity and some comments on its origin, *J. Geophys. Res.*, Vol. 74, No. 27, pp. 6777-6779.

Friedman, I., Smith, R. L., and Long, W., 1966, Hydration of Natural Glass and the Formation of Perlite, *G. S. A. Bull.*, Vol. 77, pp. 323-328.

Friedman, I., and Smith, R.L., 1960, A new dating method using obsidian; Part 1, the development of the method, *Am. Antiquity*, Vol. 25, pp. 376-522.

Friedman, I., and Smith, R.L., 1958, The deuterium content of water in some volcanic glasses, *Geochemica et Cosmochemica Acta*, Vol. 15, pp. 218-228.

Galeener, F.L., 1983, Vibrational evidence for intermediate range order in glasses, in The Structure of Non-Crystalline Materials, Gaskell, P. H., Parker, J. M., and Davis E. A., eds., Taylor & Francis, NY, pp. 337-359.

Garofalini, S. H., 1990, Molecular dynamics computer simulations of silica surface structure and adsorption of water molecules, Special Issue of the *Journal of Non-Crystalline Solids*, Vol. 120, pp. 1-12.

Goetz, A. F. H., and Rowan, L. C., 1981, Geologic Remote Sensing, Science, Vol. 211, pp. 781-791.

Haugh, G. R., 1978, Late Cenozoic, cauldron-related silicic volcanism in the Twin Peaks Area, Millard County, Utah, M.Sc. Thesis, Brigham Young University, 15p.

Heiken, G., and Woletz, K., 1987, Tephra deposits associated with silicic domes and lava flows, G. S. A. Special Paper 212, pp. 55-76.

Hildreth, W., 1979, The Bishop Tuff: evidence for the origin of compositional zonation in silicic magma chambers, G.S.A. Special Paper 180, pp. 43-75.

Hunt, G. R., and Salisbury, J. W., 1970, Visible and near-infrared spectra of minerals and rocks: I silicate minerals, Modern Geology, Vol. 1, pp. 283-300.

Iler, R. K., 1979, The Chemistry of Silica, John Wiley & Sons: New York.

Jezek, P. A., and Noble, D. C., 1978, Natural hydration and ion exchange of obsidian: an electron microprobe study, American Mineralogist, Vol. 63, pp. 266- 273.

Kadey, F. L., Jr., 1983, Perlite, Industrial Minerals and Rocks, Lefond, S.J., ed., 5th ed.,

pp. 997-1015.

Keller, W. D., and Pickett, E. E., 1954, Hydroxyl water in perlite from Superior, Arizona: American Journal of Science, No. 252, pp. 87-98.

Laursen, T., and Lanford, W. A., 1978, Hydration of obsidian, Nature, Vol. 276, No. 9, pp. 153-156.

Lipman, P. W., Rowley, P. D., Mehnert, H. H., Evans, S. H., Nash, W. P., Brown, F. H., Izett, G. A., Naeser, C. W., and Friedman, I., 1978, Pleistocene rhyolite of the mineral mountains, Utah - geothermal and archeological significance, Journal of Research, U.S. Geological Survey, Vol. 6, No. 1, pp. 133-147.

Lipman, P. W., and Friedman, I., 1975, Interaction of meteoric water with magma: an oxygen-isotope study of ash-flow sheets from southern Nevada, G. S. A. Bull., Vol. 86, pp. 695-702.

Lipman, P. W., and Christiansen, R. L., and Van Alstine, R. E., 1969, Retention of alkalis by calc-alkalic rhyolites during crystallization and hydration, The American Mineralogist, Vol. 54, pp. 286-291.

Lipman, P. W., Christiansen, R. L., and O'Connor, J. T., 1966, A compositionally zoned ash-flow sheet in southern Nevada, U. S. G. S. Professional Paper 524-F, p. F1-F47.

Lipman, P. W., 1965, Chemical comparison of glassy and crystalline volcanic rocks, U.S. G.S. Bull., 1201, pp. D1-24.

Macdonald, R., Smith, R. L., and Thomas, J. E., 1992, Chemistry of the subalkalic silicic obsidians, U. S. G. S. Professional Paper 1523, pp. 1-214.

Maniar, P. D., and Navrotsky, 1990, Energetics of high surface area silica, Special Issue of the Journal of Non-Crystalline Solids, Vol. 120, pp. 20-25.

Marakushev, A. A., and Yakovleva, E. B., 1980, On the origin of perlites, Moscow University Geol. Bull., Vol. 35, No. 1, pp. 3-17.

Marshall, R., 1961, Devitrification of Natural Glass, G. S. A. Bull., Vol. 72, pp. 1493-1520.

Meighan, C. W., 1970, Obsidian hydration rates, Science, Vol. 170, pp. 99-100.

Molnar, J., 1989, Perlite Mining in Hungary, Mining Magazine, December, pp. 498-501.

Mysen, B., 1992, Peralkalinity, Al \rightleftharpoons Substitution, and Solubility Mechanisms of H₂O in Aluminosilicate Melts, *Journal of Petrology*, Vol. 33, Part 2, pp. 347-375.

Naert, K. A., 1974, Geology, extrusion history, analysis of perlites from No Agua, New Mexico, unpublished PhD. thesis, Pennsylvania State University, State College, Pennsylvania, 223p.

Nakamoto, K., 1978, Infrared and Raman spectra of inorganic and coordination compounds, 3rd edition, Wiley, New York, 448 p.

Newman, S., Epstein, S., and Stolper, E., 1988, Water, carbon dioxide, and hydrogen isotopes in glasses from CA 1340 A. D. eruption of the Mono Craters, Craters, California: Constraints on degassing phenomena and initial volatile content, *Journal of Volcanology and Geothermal Research*, Vol. 35, pp. 75-96.

Newman, S., Stolper, E. M., and Epstein, S., 1986, Measurement of water in rhyolitic glasses: Calibration of an infrared spectroscopic technique," *American Mineralogist*, Vol. 71, pp. 1527-1541.

Noble, D. C., 1968, Stress corrosion failure and hydration of glassy silicic volcanic rocks, *American Mineralogist*, Vol. 53, pp. 1756-17759.

Nickel, B., 1987, The hydration and alteration of the perlite, pitchstone, and upper pyroclastic unit at Ruby Mountain, Nathrop, Colorado, Unpublished M.Sc. Thesis, Bowling Green State University.

Pandya, N., Muenow, D. W., and Sharma, S. K., 1992, The effect of bulk composition on the speciation of water in submarine volcanic glasses, *Geochemica et Cosmochemica Acta*, Vol. 56, pp. 1875-1883.

Paterson, M. S., 1982, The determination of hydroxyl by infrared absorption in quartz, silicate glasses and similar materials, *Bull. Miner.*, Vol. 105, pp. 20-29.

Perlaki, E. I., 1987, Volcanic glass and its relation to the Tertiary acid volcanism in the Tokaj Mountains, in Second International Conference on Natural Glasses, Prague, 1987, pp. 111-119.

Piper, J. R., 1991, The occurrence of crystalline silica in perlite; a petrographic study, in Environmental Management for the 1990's, Lootens, D. J., Greenslade, W. M., and Barker, J. M. eds., A.I. M. E., pp. 335-348.

Ross, C. S., and Smith, R. L., 1955, Water and other volatiles in volcanic glasses, *American Mineralogist*, Vol. 40, pp. 1071-1089.

Scholze, H., 1977, Glas Natur. Struktur, Eigenschaften, 2. Aufl.-Springer-Verlag: Berlin-Heidelberg-New York.

Scholze, H., 1966, Gases and water in glass, *Glass Industry*, Vol. 47, pp. 546-551, 622-628.

Scholze, H., 1960, Zur Frage der Unterscheidung zwischen H₂O- Molekeln und OH-Gruppen in Glasern und Mineralen, *Naturwissenschaften*, Vol. 47, pp. 226-227.

Scholze, H., 1959, Der Einbau des Wassers in Glasern, *Glastech. Ber.*, Vol. 32, pp. 81-88, 142-145, 278-281.

Sheridan, M. F., 1979, Emplacement of Pyroclastic Flows: A Review, *G. S. A. Special Paper* 180, pp. 125 - 136.

Stevenson, C. M., Knaus, E., Mazer, J. J., and Bates, J. K., 1993, Homogeneity of water content in obsidian from Coso Volcanic Field: Implications for obsidian hydration dating, *Geoarchaeology: An International Journal*, Vol. 8, No. 5, pp. 371-384.

Stolper, E., 1989, Temperature dependence of the speciation of water in rhyolitic melts and glasses, *American Mineralogist*, Vol. 74, pp. 1247-1257.

Stolper, E., 1982, Water in silicate glass: An infrared spectroscopic study, *Contributions to Mineralogy and Petrology*, Vol. 81, pp. 1-17.

Sykes, D., and Kubicki, J. D., 1993, A model for solubility mechanisms in albite melts from infrared spectroscopy and molecular orbital calculations, *Geochemica et Cosmochemica Acta* Vol. 57, pp. 1039-1052.

Taylor, B. E., Eichelberger, J. C., and Westrich, H. R., 1983, Hydrogen isotopic evidence of rhyolitic magma degassing during shallow intrusion and eruption, *Nature*, Vol. 306, December, pp. 541-545.

Tossell, J. A., 1990, Calculations of NMR shieldings and other properties for three and five coordinate Si, and some siloxene and boroxyl ring complexes, *Special Issue of the Journal of Non-crystalline Solids*, Vol. 120, pp. 13-19.

Whitson, D., 1982, *Geology of the Perlite Deposit at No Agua Peaks, New Mexico*, New Mexico Bureau of Mines & Mineral Resources, Circ. 182, pp. 89- 95.

Wu, C. K., 1980, Nature of incorporated water in hydrated silicate glasses, *Journal of the American Ceramic Society*, Vol. 63, No. 7-8, pp. 453-457.

Zemann, J., 1987, What is glass?, Second International Conference on Natural Glasses, Prague, 1987, pp.35-40.

Zielinski, R. A., Lipman, P. W., and Millard, H. T. Jr., 1977, Minor element abundances in obsidian, perlite, and felsite of calc-alkalic rhyolites, *American Mineralogist*, Vol. 72, pp. 426-437.